Supporting Information

Synthesis and electron-transporting properties of phenazine bisimides

Keita Tajima,[1] Taito Moribe,[1] Kyohei Matsuo,[2] Hiroko Yamada,[2] Shu Seki,[3] Seiya Yokokura[4], Toshihiro Shimada[4], Norihito Fukui,[1,5*] and Hiroshi Shinokubo[1*]

[1]Department of Molecular and Macromolecular Chemistry, Graduate School of Engineering Nagoya University, Furo-cho, Chikusa-ku, Nagoya 464-8603 (Japan)

[2]Institute of Chemical Research, Kyoto University, Gokasho, Uji, Kyoto 611-0011, Japan

[3]Department of Molecular Engineering, Graduate School of Engineering, Kyoto University, Nishikyo-ku, Kyoto 615-8510, Japan

[4]Graduate School of Chemical Sciences and Engineering, Hokkaido University, Kita 13 Nishi 8, Kita-ku, Sapporo 060-8628, Japan

[5]PRESTO, Japan Science and Technology Agency (JST), Kawaguchi, Saitama 332-0012 (Japan)

E-mail: hyamada@scl.kyoto-u.ac.jp, seki@moleng.kyoto-u.ac.jp, fukui@chembio.nagoya-u.ac.jp, hshino@chembio.nagoya-u.ac.jp

Table of Contents

1. Instrumentation and materials 3
2. Experimental procedures and compound data 5
3. NMR spectra 11
4. Mass spectra 28
5. Crystal data 37
6. Electron-transporting behavior 39
7. TRMC measurement 45
8. DFT calculations 48
9. Optical properties 53
10. Redox properties 54
11. References 55

1. Instrumentation and materials

^{1}H NMR (500 MHz), ^{13}C NMR (126 MHz), and ^{19}F NMR (471 MHz) spectra were recorded on a Bruker AVANCE III HD and JEOL JNM-ECA600II spectrometer. Chemical shifts were reported as the delta scale in ppm relative to $CHCl_3$ (δ = 7.26 ppm), DMSO-d_6 (δ = 2.50 ppm), and tetrachloroethane-d_2 (δ = 7.16 ppm), for ^{1}H NMR, and $CDCl_3$ (δ = 77.16 ppm), DMSO-d_6 (δ = 39.52 ppm), and tetrachloroethane-d_2 (δ = 73.77 ppm) for ^{13}C NMR. Preparative separations were performed by silica gel column chromatography (Wako gel® C-400 and FUJISILYSIA CHROMATOREX NH−DM1020). High-resolution atmospheric pressure chemical ionization time-of-flight (APCI-TOF) and electrospray ionization time-of-flight (ESI-TOF) mass spectra were taken on a Bruker micrOTOF instrument using a positive or negative ionization mode. High-resolution matrix-assisted laser desorption and ionization time-of-flight (MALDI-TOF) mass spectra were taken on a Bruker autoflex max using a positive ionization mode. Redox potentials were measured using cyclic voltammetry on an ALS electrochemical analyzer model 612C. Powder X-ray diffraction (XRD) data were collected with Cu Kα radiation using Rigaku R-AXIS-IV and R-AXIS-VII X-ray imaging plate detectors. The Hirshfeld surface analyses were performed using the Crystal Explorer software.[1] Out-of-plane XRD measurements of the thin films were performed using a Rigaku RINT-TTR III/NM X-ray diffractometer with a Cu Kα source (λ = 1.5418 Å) in the 2θ scan mode at a fixed incidence angle of 0.58°. Photoelectron yield spectroscopy measurement was performed using a Riken Keiki AC-3 photoelectron spectrometer. The atomic force microscope images were obtained using Shimadzu SPM-9700 in the tapping mode. All calculations were carried out using the *Gaussian 16* programs.[2] Calculations were performed with Becke's three-parameter hybrid exchange functional and the Lee–Yang–Parr correlation functional (B3LYP),[3] or hybrid exchange-correlation functional using the Coulomb-attenuating method (CAM-B3LYP),[4] or Perdew–Burke–Ernzerhof hybrid exchange-correlation functional (PBEPBE).[5] X-ray data were obtained using a Rigaku CCD diffractometer (Saturn 724 with MicroMax-007) with Varimax Mo optics. The structures were solved using a direct method (SHELXT) and refined by a full-matrix least-squares method on F^2 for all reflections using the programs of SHELXL-2014. All nonhydrogen atoms were refined with anisotropic displacement parameters. The hydrogen atoms were placed in idealized positions and refined as riding models with the relative isotropic displacement parameters. Crystallographic data have been deposited with the Cambridge Crystallographic Data Centre as a supplementary publication. The oil bath was used as the heat source for reactions under heating conditions. Dry 1,4-dioxane was prepared

using GlassContour™ solvent purification systems. Diethyl 4-nitrophthalate **7** was synthesized according to the literature.[6] Unless otherwise noted, materials obtained from commercial suppliers were used without further purification.

2. Experimental procedures and compound data

Diethyl 4-aminophthalate 8

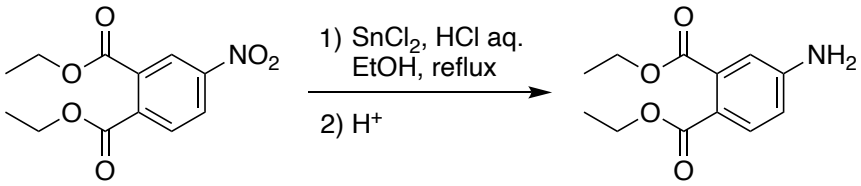

Diethyl 4-nitrophthalate **7** (7.94 g, 25.6 mmol) and ethanol (150 mL) were placed in a 300 mL round-bottomed flask. The mixture was stirred at room temperature for 3 min. A solution of $SnCl_2$ (19.1 g, 101 mmol) in conc. HCl aq. (25 mL) was added slowly to the mixture. The mixture was refluxed for 2 h. The resulting mixture was cooled to 0 °C using ice bath. Then, the reaction was quenched by the addition of an aqueous $NaHCO_3$ solution. The reaction mixture was extracted with AcOEt. The organic phase was separated, washed with water and brine, and dried over Na_2SO_4. After removing the solvent, washing the residue with hexane afforded **8** (5.44 g, 23.0 mmol, 90%) as a pale-yellow solid.

The characterization data matched with the previous report.[6] ^{1}H NMR (500 MHz, $CDCl_3$, 298 K): δ = 7.70 (d, J = 8.5 Hz, 1H), 6.70 (d, J = 2.4 Hz, 1H), 6.65 (dd, J_1 = 8.5 Hz, J_2 = 2.4 Hz, 1H), 4.34 (q, J = 7.2 Hz, 2H), 4.28 (q, J = 7.1 Hz, 2H), 4.16 (s, 2H), 1.34 (t, J = 7.2 Hz, 3H), 1.32 (t, J = 7.1 Hz, 3H) ppm; ^{13}C NMR (126 MHz, $CDCl_3$, 298 K): δ = 169.4, 166.4, 150.0, 136.7, 132.0, 118.6, 115.0, 113.4, 61.7, 61.0, 14.3, 14.2 ppm; HRMS (APCI-TOF, positive mode): $[M+Na]^+$ Calcd for $C_{12}H_{15}NO_4Na$ 260.0893; Found 260.0902.

Diethyl 4-amino-5-iodophthalate 9

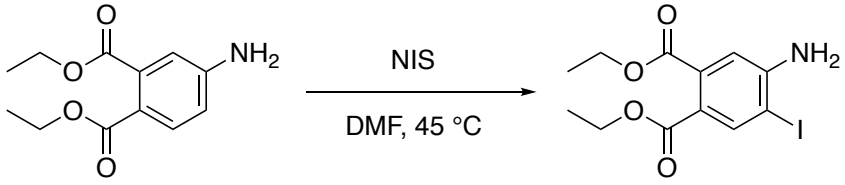

Compound **8** (1.02 g, 4.20 mmol) and DMF (26 mL) were placed in a 100 mL round-bottomed flask. The mixture was stirred at room temperature for 3 min. NIS (1.94 g, 8.61 mmol) was added in one portion. The mixture was stirred at 45 °C for 11 h under light-shielded conditions. The resulting mixture was cooled to 0 °C using ice bath. Then, the reaction was quenched by the addition of an aqueous $Na_2S_2O_3$ solution. The reaction mixture was extracted with toluene. The organic phase was separated, washed with water and brine, and dried over Na_2SO_4. After

removing the solvent, the residue was purified by amino-functionalized silica gel column chromatography (eluent: AcOEt/hexane = 1/4 to 1/1). After removal of the solvent *in vacuo*, crystallization by scratching the supercooling oil afforded compound **9** (885 mg, 2.44 mmol, 57%) as a pale-yellow solid.

^{1}H NMR (500 MHz, $CDCl_3$, 298 K): δ = 8.16 (s, 1H), 6.77 (s, 1H), 4.65 (s, 2H), 4.32 (q, J = 7.2 Hz, 2H), 4.28 (q, J = 7.2 Hz, 2H), 1.33 (t, J = 7.2 Hz, 3H), 1.32 (t, J = 7.2 Hz, 3H) ppm; ^{13}C NMR (126 MHz, $CDCl_3$, 298 K): δ = 168.6, 165.0, 150.1, 141.1, 136.3, 119.9, 112.6, 83.5, 61.9, 61.3, 14.3, 14.1 ppm; HRMS (APCI-TOF, positive mode): $[M+Na]^+$ Calcd for $C_{12}H_{14}NO_4INa$ 385.9860; Found 385.9877.

Phenazine-2,3,6,7-tetracarboxylic acid tetraethyl ester 10

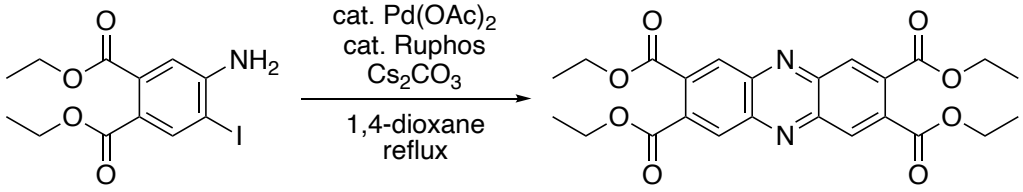

A mixture of compound **9** (873 mg, 2.4 mmol), $Pd(OAc)_2$ (53.4 mg, 238 μmol), Ruphos (225 mg, 483 μmol), and Cs_2CO_3 (2.36 g, 7.23 mmol) was prepared in an-argon filled glove box. Then, the mixture was removed from the glove box, and dry 1,4-dioxane (24 mL) was added. The mixture was refluxed for 6 h under argon in the dark. The reaction mixture was cooled to room temperature. The resulting mixture was filtered on a Celite pad and washed with $CHCl_3$. After removing the solvent, the residue was purified by amino-functionalized silica gel column chromatography (eluent: AcOEt/hexane = 1/9 to 1/1). After the removal of the solvent *in vacuo*, the residue was washed by hexane. Compound **10** (351 mg, 751 μmol, 63%) was obtained as a yellow solid.

^{1}H NMR (500 MHz, $CDCl_3$, 298 K): δ = 8.66 (s, 4H), 4.49 (q, J = 7.2 Hz, 8H), 1.45 (t, J = 7.2 Hz, 12H) ppm; ^{13}C NMR (126 MHz, $CDCl_3$, 298 K): δ = 166.3, 144.3, 134.3, 132.1, 62.5, 14.3 ppm; HRMS (ESI-TOF, positive mode): $[M+Na]^+$ Calcd for $C_{24}H_{24}N_2O_8Na$ 491.1425; Found 491.1433.

Phenazine-2,3,6,7-tetracarboxylic acid 11

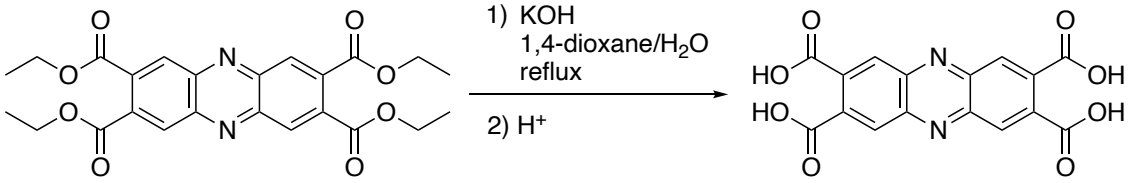

Compound **10** (351 mg, 751 μmol), 1,4-dioxane (15 mL), and water (7.5 mL) were placed in a 100 mL round-bottomed flask. The mixture was stirred at room temperature for 3 min. KOH (1.94 g, 8.61 mmol) was added with one portion. The mixture was refluxed for 11 h under light-shielded conditions. The resulting mixture was cooled to room temperature. Then, 2 M HCl aq. (50 mL) was added. The mixture was stirred at room temperature for 16 h under light-shielded conditions. The resulting mixture was filtered and washed with water. Compound **11** (232 mg, 652 μmol, 87%) was obtained as an off-white solid.

^{1}H NMR (500 MHz, DMSO-d_6, 298 K): δ = 8.55 (s, 4H) ppm (The signal of carboxylic acid was hardly observed, probably due to the hydrogen bonding with solvents and spontaneous proton exchange reactions.); ^{13}C NMR (126 MHz, DMSO-d_6, 298 K): δ = 167.5, 143.7, 135.3, 130.8 ppm; HRMS (ESI-TOF, negative mode): $[M–H]^-$ Calcd for $C_{16}H_7N_2O_8$ 355.0208; Found 355.0212.

Phenazine-2,3,6,7-tetracarboxylic dianhydride 12

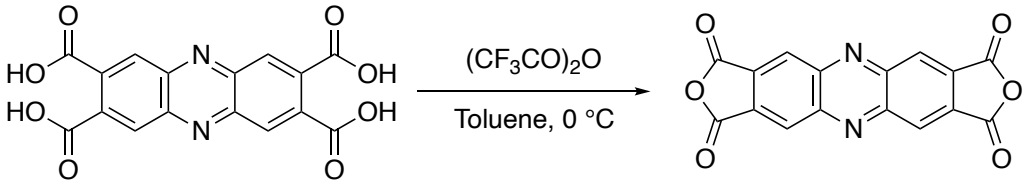

Compound **11** (232 mg, 652 μmol) and toluene (65 mL) were placed in a 100 mL round-bottomed flask. The mixture was sonicated for 1 min and stirred at 0 °C for 3 min. Trifluoroacetic anhydride (1.8 mL, 13 mmol) was added slowly to the mixture. The mixture was stirred at 0 °C for 2 h in the dark. The resulting mixture was filtered and washed with toluene and hexane. Compound **12** (168 mg, 523 μmol, 80%) was obtained as a yellow solid. Further purification was not conducted in this step.

^{1}H and ^{13}C NMR spectra were not obtained due to the poor solubility of the product and the low stability toward moisture. HRMS (MALDI-TOF, positive mode): $[M+H]^+$ Calcd for $C_{16}H_5N_2O_6$ 321.0142.1425; Found 321.0139.

***N*,*N*'-Bis(3,5-di-*tert*-butylphenyl)phenazine-2,3,6,7-tetracarboximide 4a**

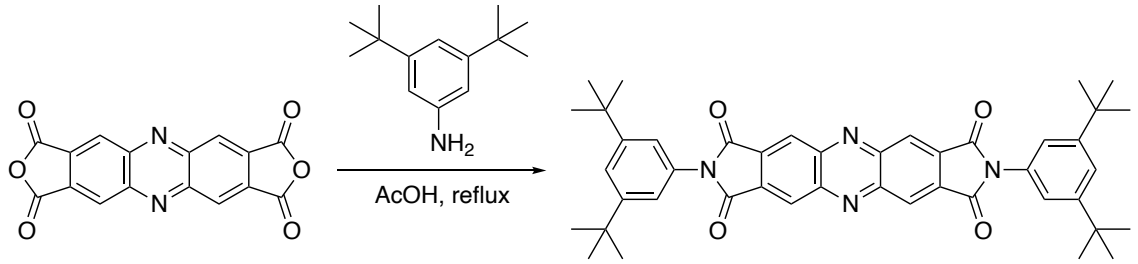

Compound **12** (160 mg, 499 μmol), 3,5-di-*tert*-butylaniline (306 mg, 1.49 mmol), and AcOH (25 mL) were placed in a 100 mL round-bottomed flask. The mixture was refluxed for 15 h under light-shielded conditions. The reaction mixture was cooled to room temperature. The resulting mixture was filtered and washed with 2 M HCl aq. and water. The solid was dried under reduced pressure. After removing the solvent, the residue was purified by silica gel column chromatography (eluent: CH_2Cl_2). After the removal of the solvent *in vacuo*, the residue was washed with hexane. Compound **4a** (217 mg, 312 μmol, 63%) was obtained as a yellow solid.

^{1}H NMR (500 MHz, $CDCl_3$, 298 K): δ = 8.91 (s, 4H), 7.54 (t, J = 1.7 Hz, 2H), 7.32 (t, J = 1.7 Hz, 4H), 1.39 (s, 36H) ppm; ^{13}C NMR (126 MHz, $CDCl_3$, 298 K): δ = 165.6, 152.2, 146.1, 132.7, 130.8, 127.5, 123.3, 121.0, 35.3, 31.5 ppm; HRMS (APCI-TOF, negative mode): $[M]^-$ Calcd for $C_{44}H_{46}N_4O_4$ 694.3514; Found 694.3514.

***N*,*N*'-biscyclohexylphenazine-2,3,6,7-tetracarboximide 4b**

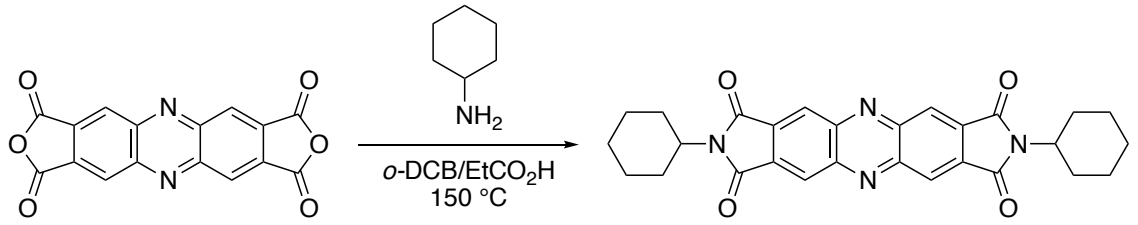

Compound **12** (63.9 mg, 199 μmol) and *o*-dichlorobenzene (8 mL) were placed in a 50 mL round-bottomed flask. The mixture was sonicated for 1 min. Cyclohexylamine (70 μL, 0.61 mmol) was added to the mixture. The mixture was stirred at 150 °C for 12 h under light-shielded conditions. Propionic acid (2 mL) was added to the mixture. The crude mixture was stirred at 150 °C for 48 h under light-shielded conditions. The reaction mixture was cooled to room temperature and quenched by aqueous $NaHCO_3$ solution. The resulting mixture was filtered and washed with water and MeOH. Compound **4b** (58.4 mg, 122 μmol, 61%) was obtained as a crystalline yellow solid.

^{1}H NMR (500 MHz, $CDCl_3$, 298 K): δ = 8.74 (s, 4H), 4.29 (tt, J_1 = 18.5 Hz, J_2 = 3.9 Hz, 2H), 2.32 (qd, J_1 = 12.3 Hz, J_2 = 3.4 Hz, 4H), 1.93 (m, 4H), 1.82 (m, 4H), 1.75 (m, 2H), 1.43 (qt, J_1 = 13.1 Hz, J_2 = 3.4 Hz, 4H), 1.34 (tt, J_1 = 12.8 Hz, J_2 = 3.2 Hz, 2H) ppm; ^{13}C NMR (126 MHz, $CDCl_3$, 298 K): δ = 166.2, 145.8, 132.7, 126.5, 52.1, 29.6, 25.9, 25.1 ppm; HRMS (APCI-TOF, negative mode): $[M]^-$ Calcd for $C_{28}H_{26}N_4O_4$ 482.1949; Found 482.1970.

***N,N'*-bis(2,2,3,3,4,4,4-heptafluorobutyl)phenazine-2,3,6,7-tetracarboximide 4c**

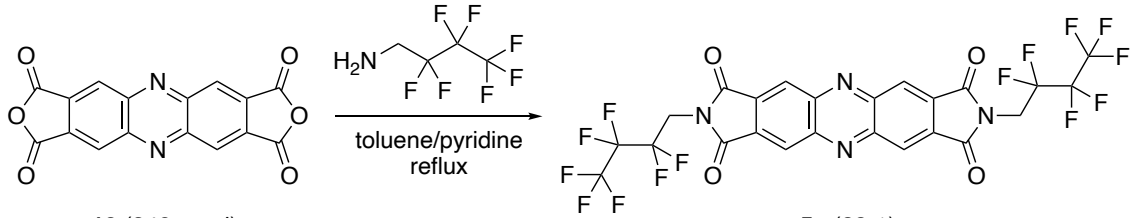

Compound **12** (111 mg, 348 μmol), toluene (14 mL), and pyridine (3.5 mL) were placed in a 50 mL round-bottomed flask. 2,2,3,3,4,4,4-Heptafluorobutylamine (0.14 mL, 1.1 mmol) was added slowly to the mixture. The mixture was refluxed for 14 h under light-shielded conditions. The reaction mixture was cooled to room temperature. The resulting mixture was filtered and washed with MeOH. The crude solid was recrystallized from *o*-DCB at 140 °C. The precipitates were filtered and washed with DCM. Compound **4c** (52.6 mg, 77.0 μmol, 22%) was obtained as a crystalline yellow solid.

^{1}H NMR (500 MHz, $(CD_2Cl_2)_2$, 403 K): δ = 8.97 (s, 4H), 4.59 (t, J = 14.8 Hz, 4H) ppm; ^{13}C NMR (126 MHz, $(CD_2Cl_2)_2$, 403 K): δ = 164.1, 145.7, 131.9, 127.8, 38.1 (t, J = 50.3 Hz) ppm; ^{19}F NMR (471 MHz, $(CD_2Cl_2)_2$, 403 K): δ = –79.9 (6F), –114.6 (4F), –126.4 (4F) ppm; HRMS (APCI-TOF, negative mode): $[M]^-$ Calcd for $C_{24}H_8F_{14}N_4O_4$ 682.0317; Found 682.0332.

***N,N'*-dihydrophenazine bisimide 13**

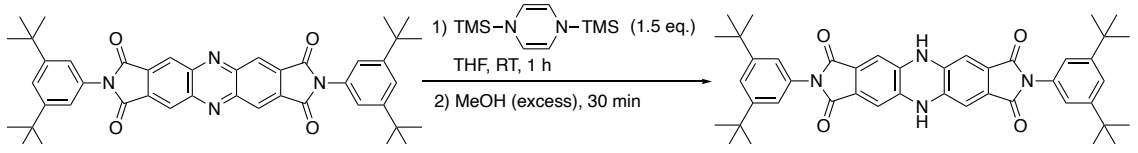

In an argon-filled glovebox, compound **4a** (19.1 mg, 27.5 μmol), 1,4-bis(trimethylsilyl)-1,4-dihydropyrazine (9.4 mg, 42 μmol), and dry THF (2.5 mL) were placed in an 8 mL vial. The mixture was stirred at room temperature for 1 h. MeOH (1 mL) was added to the reaction mixture. The precipitates were filtrated and washed with methanol, affording compound **13** (17.1 mg, 24.6 μmol, 89%) as a brown solid. The obtained solid was purified by silica gel column

chromatography (eluent: CH_2Cl_2/AcOEt = 20/1) for photophysical measurements.

^{1}H NMR (500 MHz, DMSO-d_6, 293 K): δ = 8.82 (s, 2H, The signal was weakened by the addition of D_2O.), 7.39 (s, br, 2H), 7.12 (s, br, 4H), 6.22 (s, 4H), 1.27 (s, 36H) ppm; ^{13}C NMR (126 MHz, DMSO-d_6, 293 K): δ = 166.6, 150.8, 138.9, 131.6, 126.1, 121.2, 105.1, 34.6, 31.1 ppm; HRMS (ESI-TOF, negative mode): $[M–H]^-$ Calcd. for $C_{44}H_{47}N_4O_4$ 695.3603; Found 695.3575.

Oxidation of *N,N'*-dihydrophenazine bisimide 13

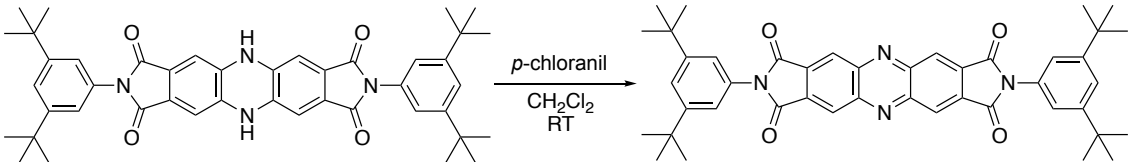

Dihydrophenazine bisimide **13** (3.68 mg, 5.28 μmol) and CH_2Cl_2 (5 mL) were placed in a 50 mL round-bottomed flask. The mixture was stirred at room temperature for 3 min. Then, *p*-chloranil (2.77 mg, 11.3 μmol) was added to the mixture. The mixture was stirred for 5 min at room temperature. After removing the solvent, the residue was purified by silica gel column chromatography (eluent: CH_2Cl_2/AcOEt = 50/1). After the removal of the solvent *in vacuo*, compound **4a** (1.89 mg, 2.72 μmol, 51%) was obtained as a yellow solid.

3. NMR spectra

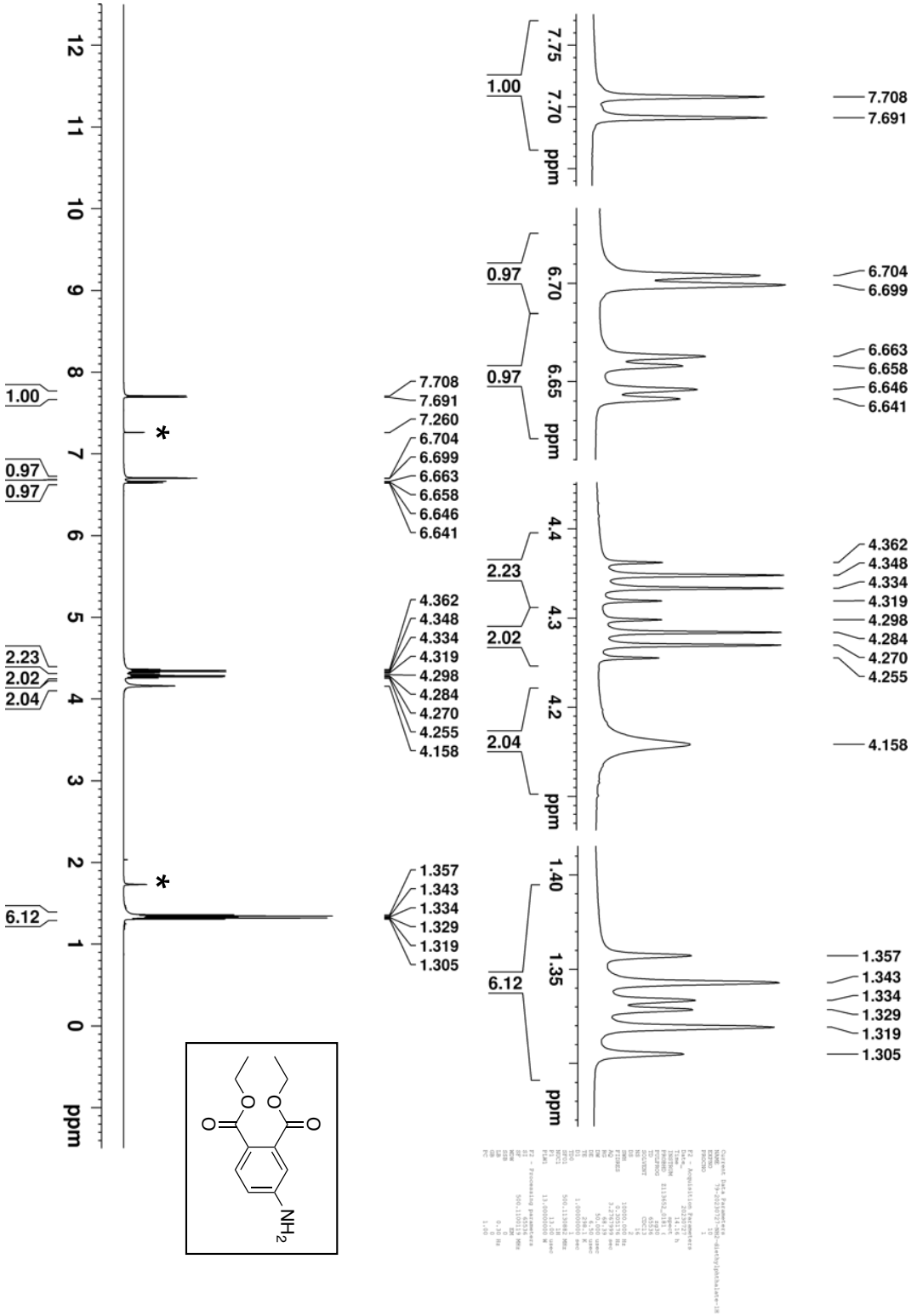

Figure S1. ^{1}H NMR spectrum of **8** in $CDCl_3$ at 25 °C. *Residual solvents.

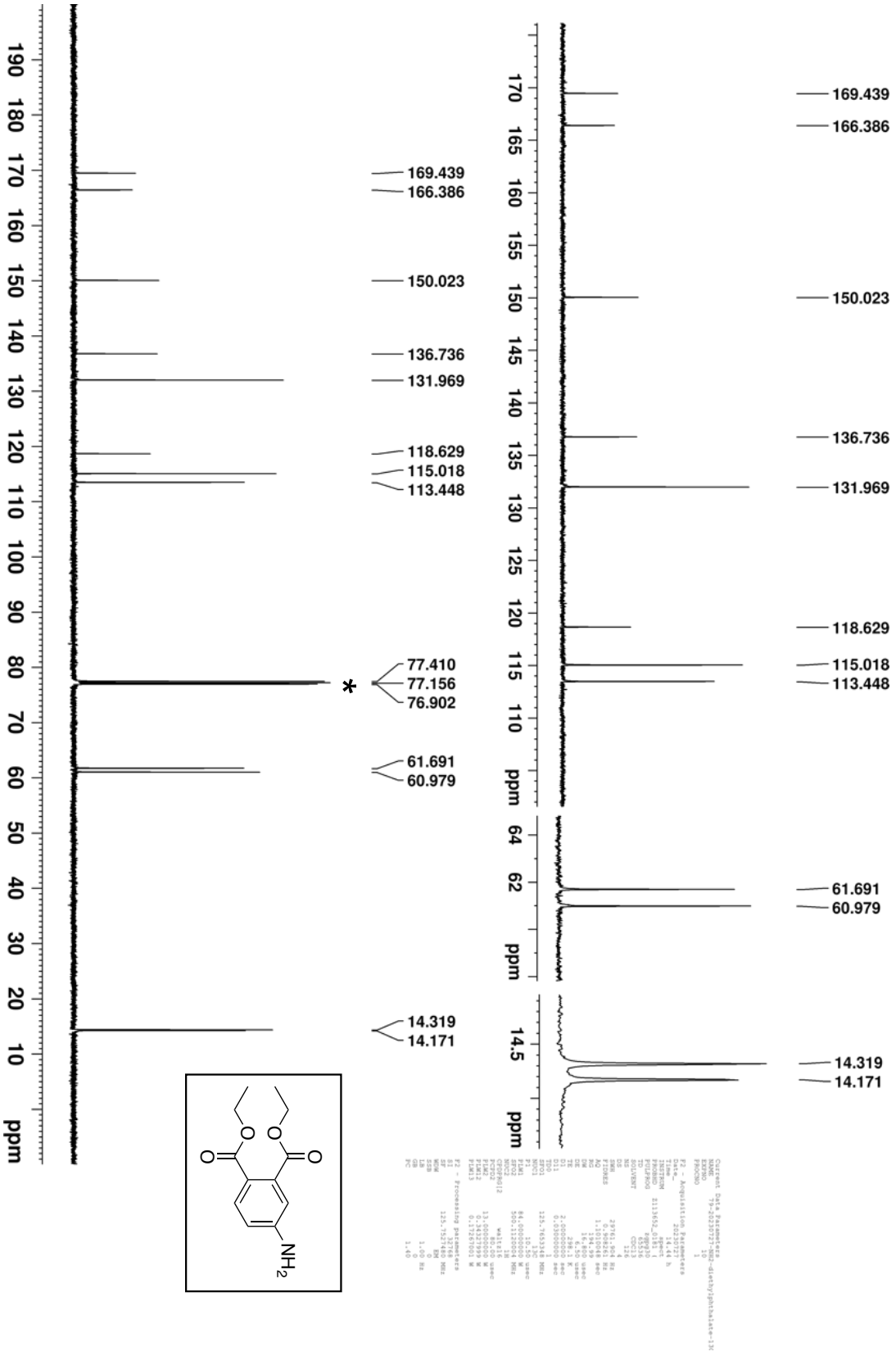

Figure S2. ^{13}C NMR spectrum of **8** in $CDCl_3$ at 25 °C. *Residual solvent.

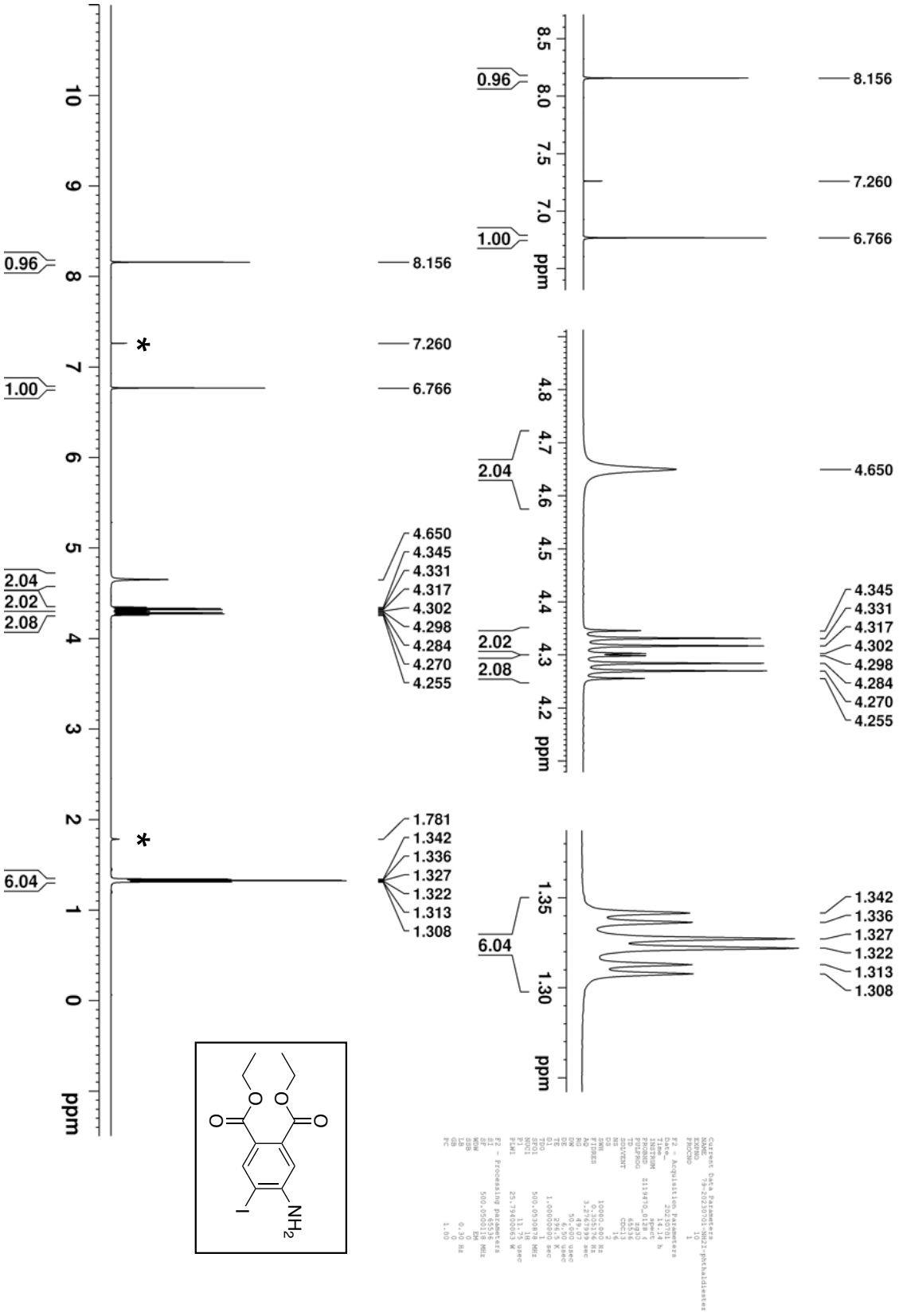

Figure S3. ^{1}H NMR spectrum of **9** in $CDCl_3$ at 25 °C. *Residual solvents.

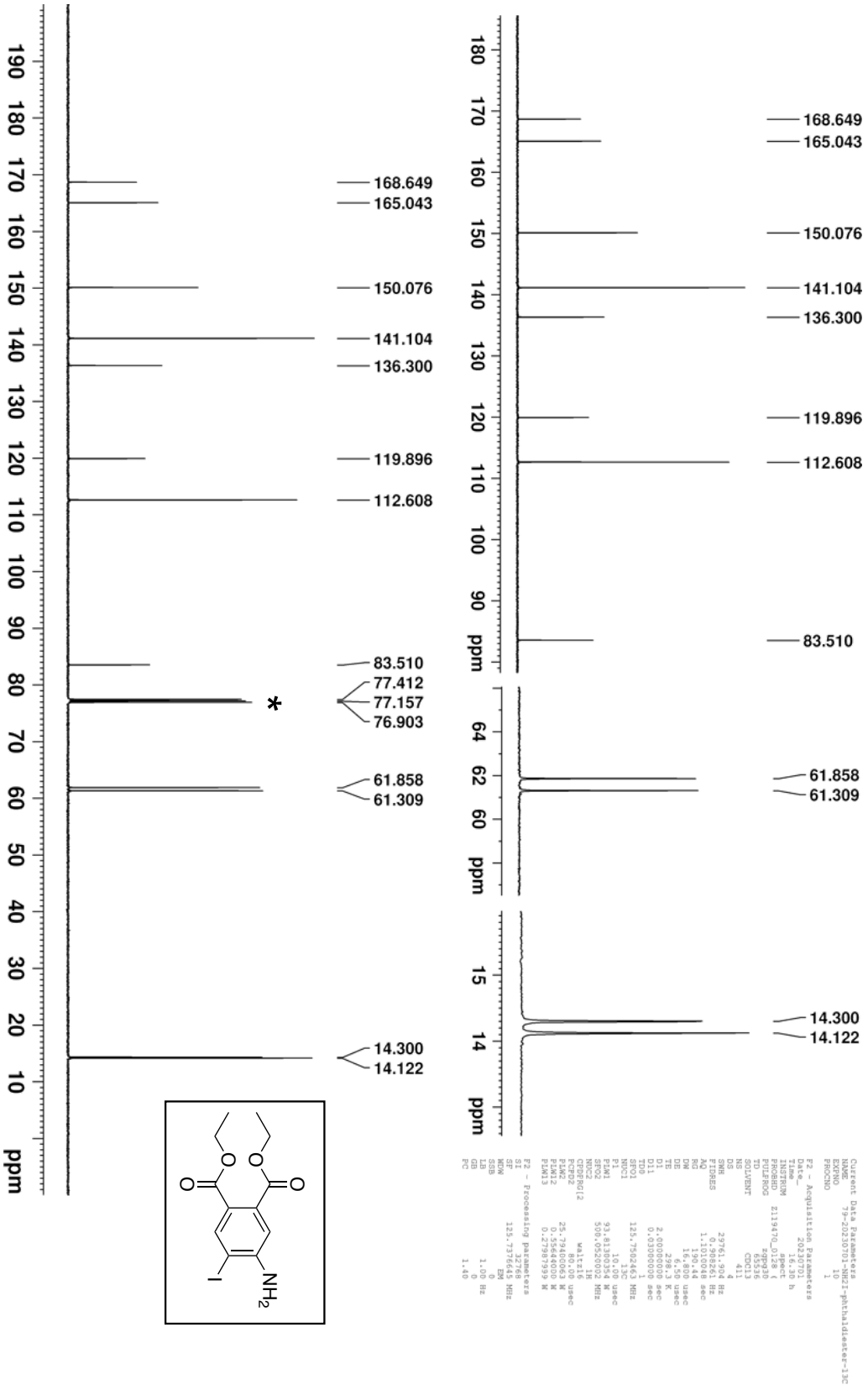

Figure S4. ^{13}C NMR spectrum of **9** in $CDCl_3$ at 25 °C. *Residual solvent.

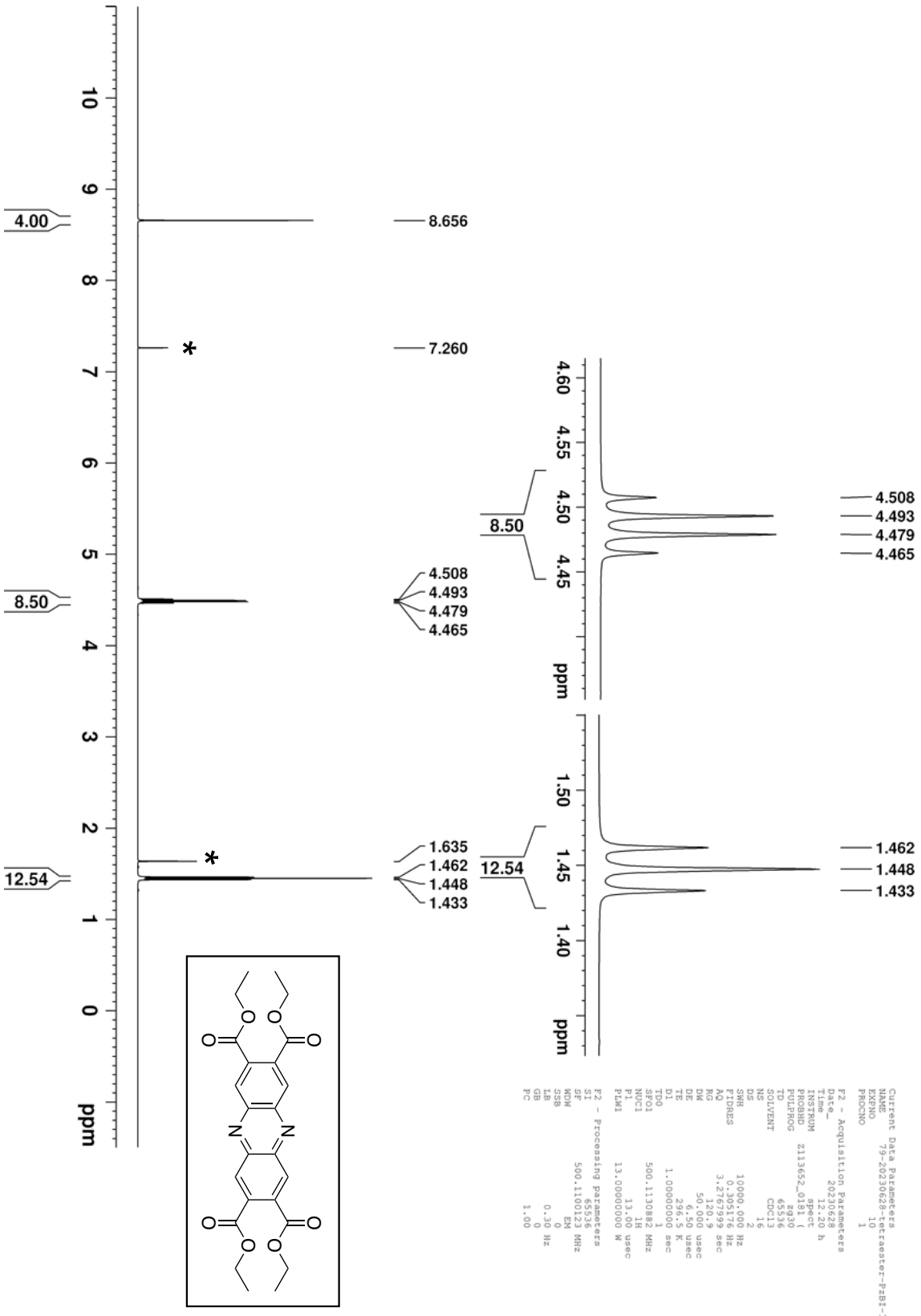

Figure S5. ^{1}H NMR spectrum of **10** in $CDCl_3$ at 25 °C. *Residual solvents.

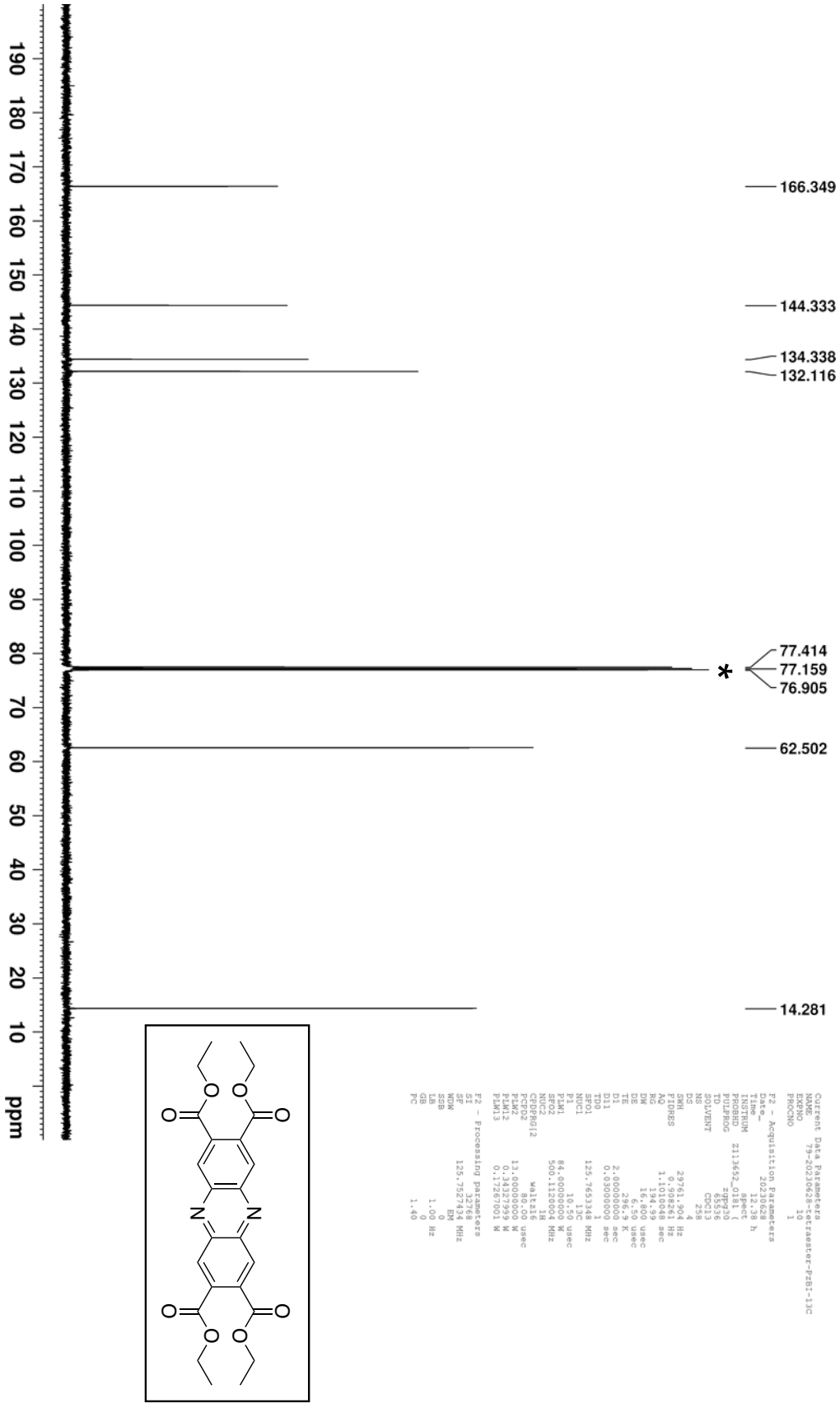

Figure S6. ^{13}C NMR spectrum of **10** in $CDCl_3$ at 25 °C. *Residual solvent.

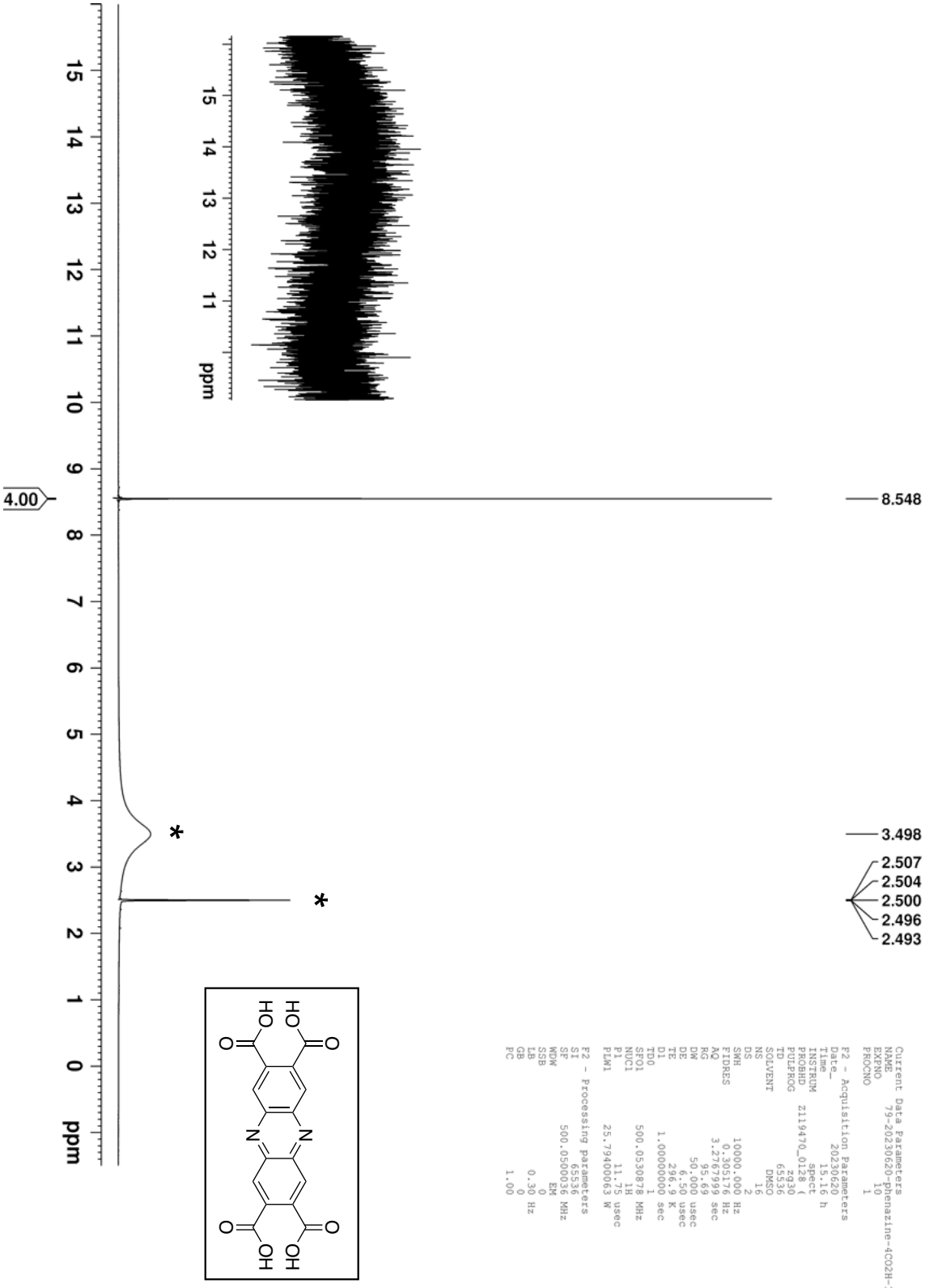

Figure S7. ^{1}H NMR spectrum of **11** in DMSO-d_6 at 25 °C. *Residual solvents.

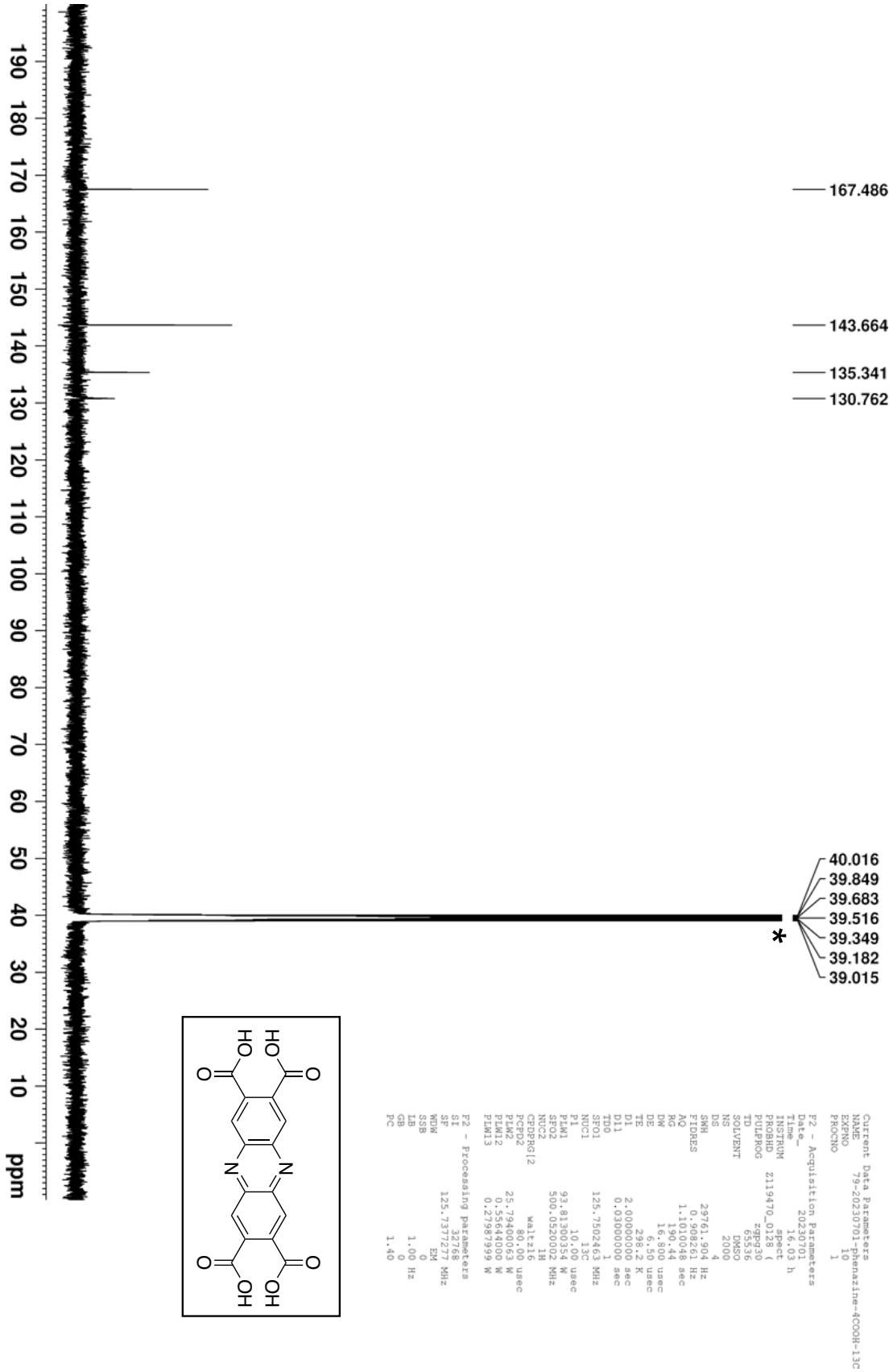

Figure S8. ^{13}C NMR spectrum of **11** in DMSO-d_6 at 25 °C. *Residual solvent.

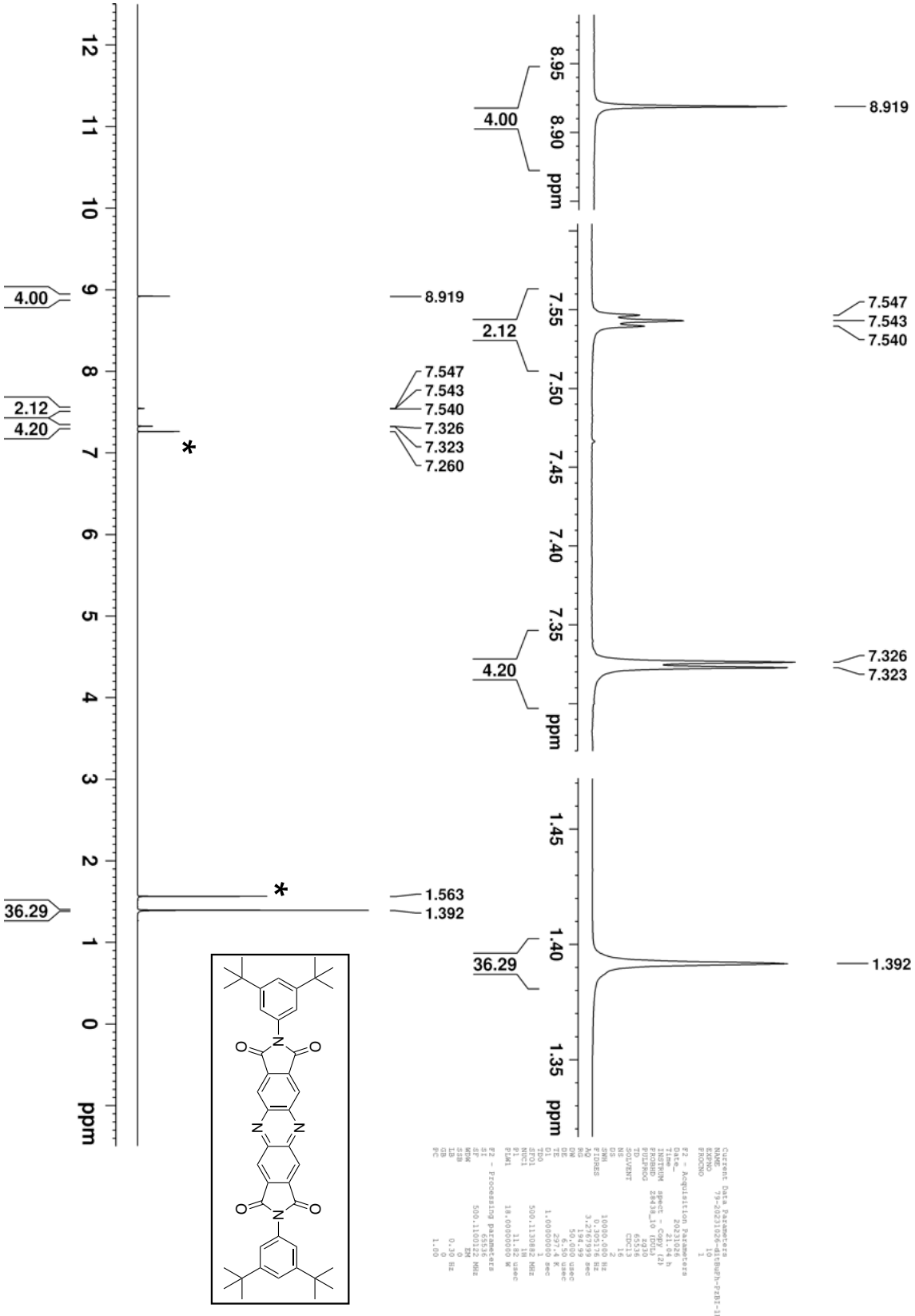

Figure S9. ^{1}H NMR spectrum of **4a** in $CDCl_3$ at 25 °C. *Residual solvents.

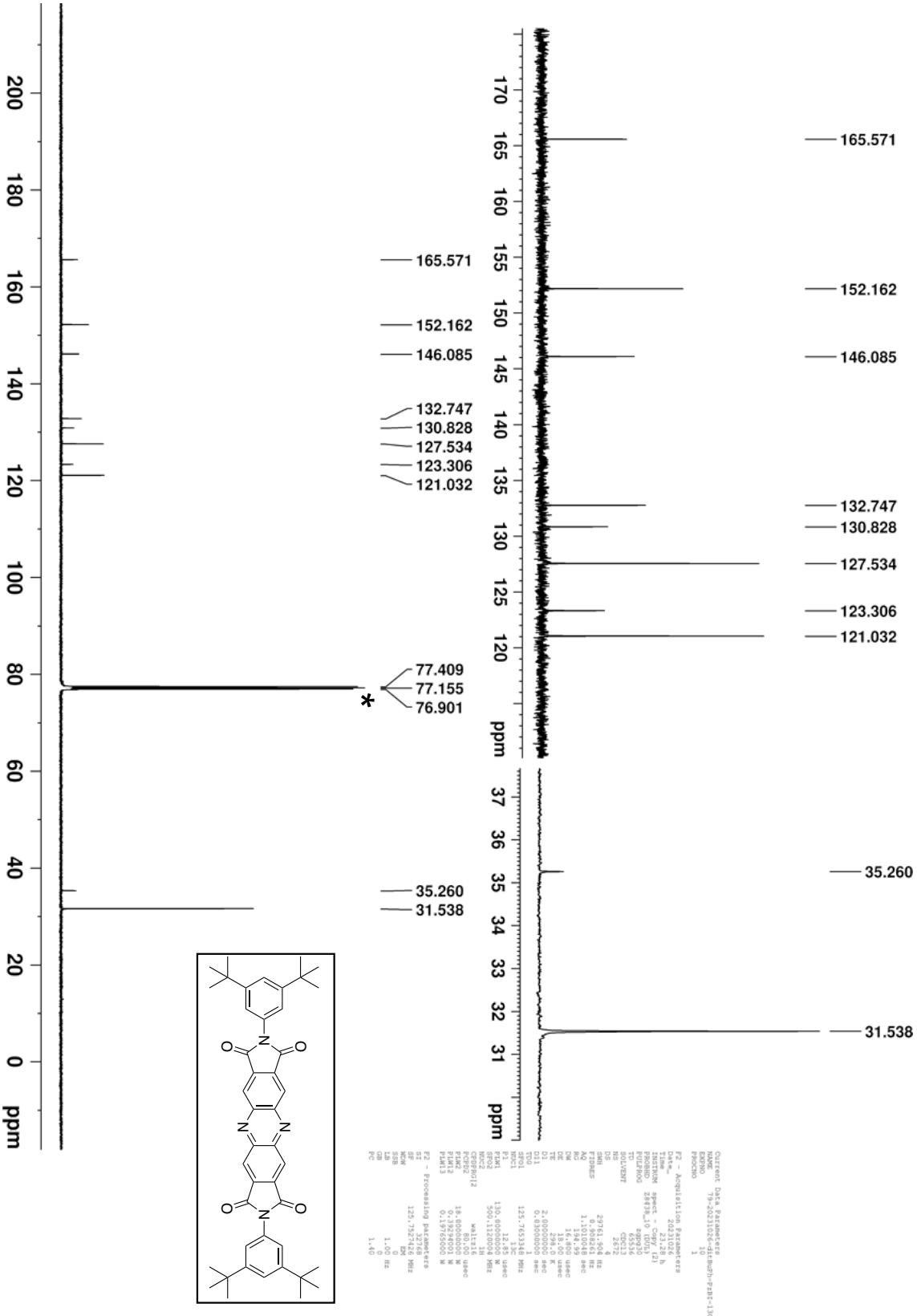

Figure S10. ^{13}C NMR spectrum of **4a** in $CDCl_3$ at 25 °C. *Residual solvent.

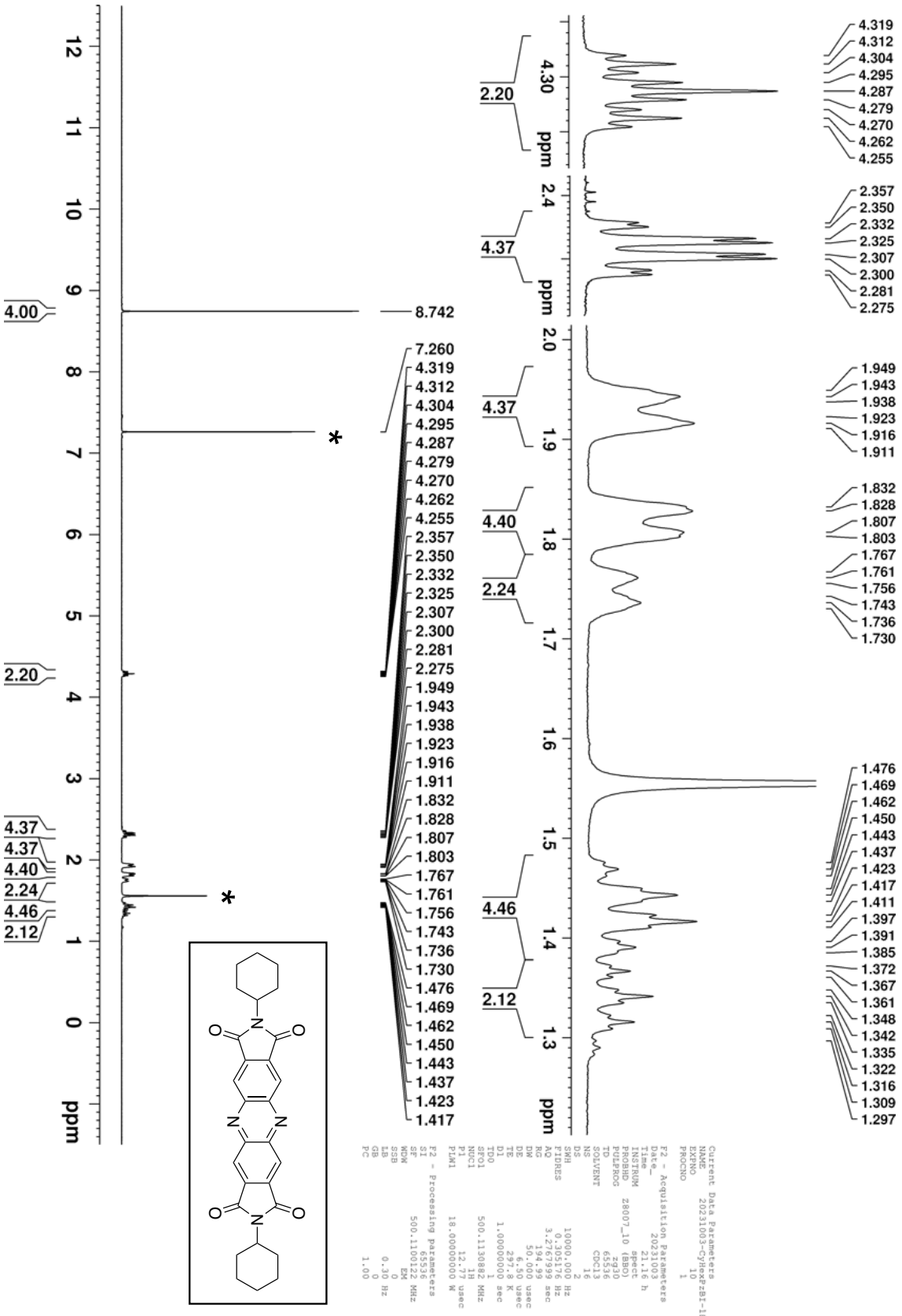

Figure S11. ^{1}H NMR spectrum of **4b** in $CDCl_3$ at 25 °C. *Residual solvents.

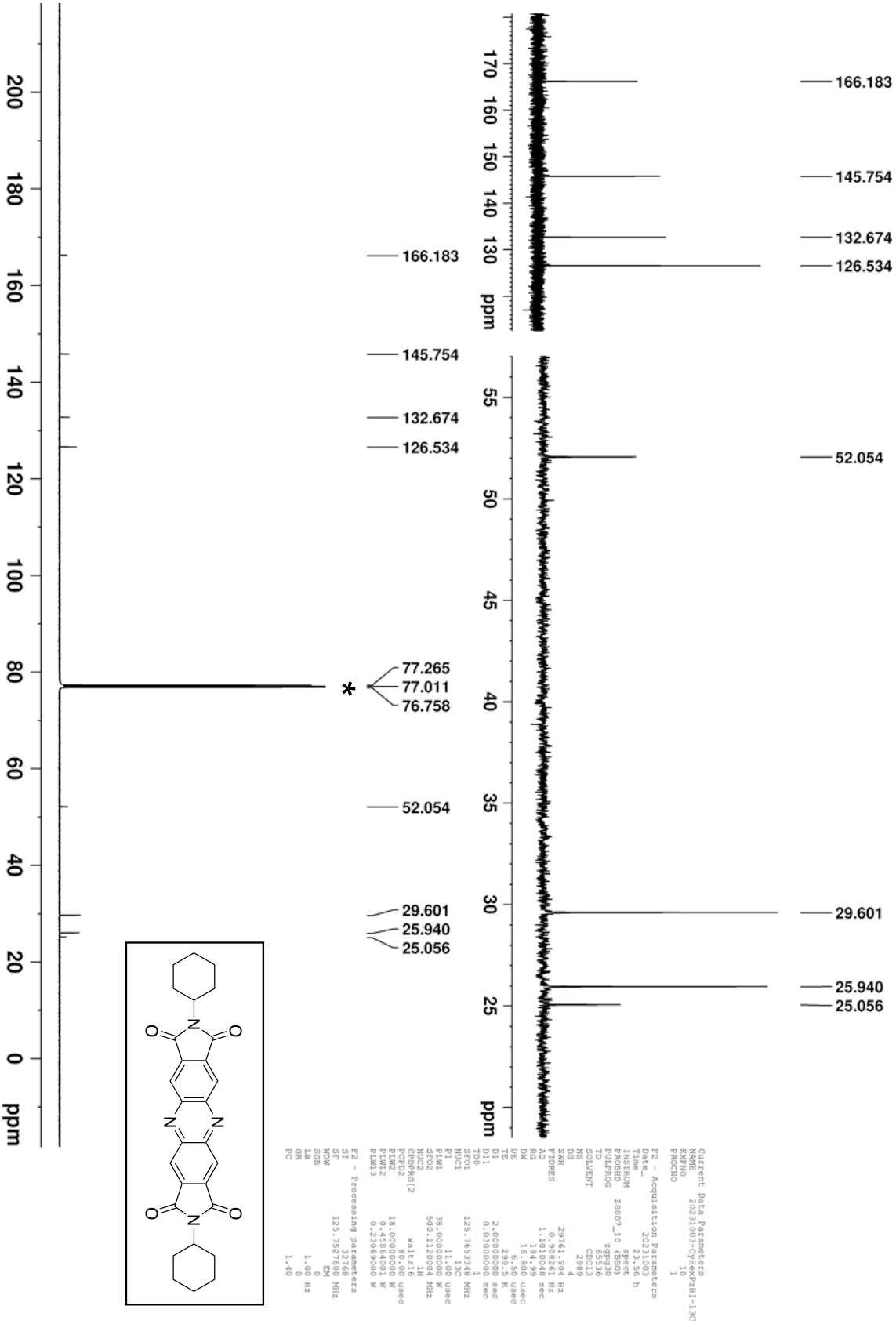

Figure S12. ^{13}C NMR spectrum of **4b** in $CDCl_3$ at 25 °C. *Residual solvent.

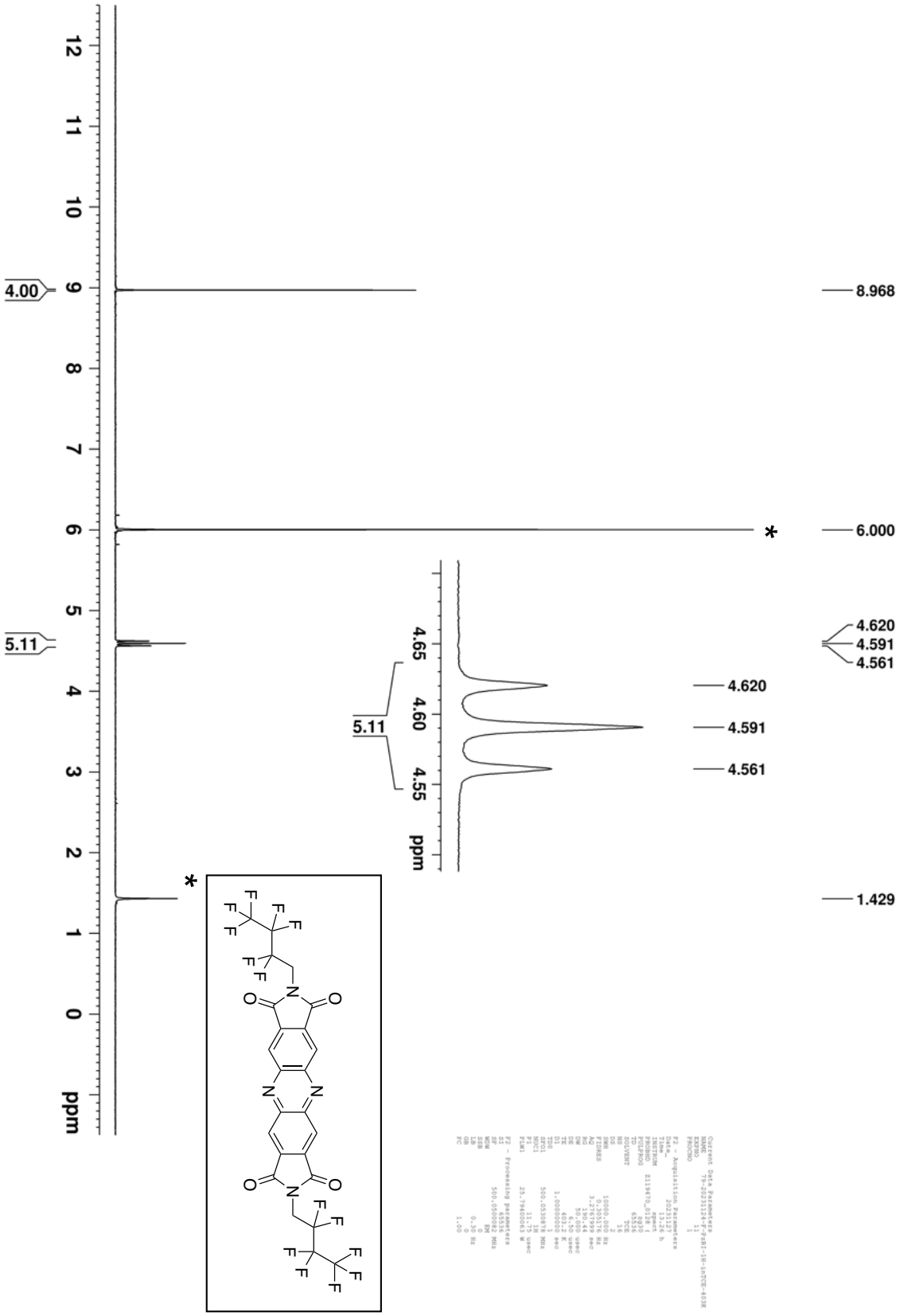

Figure S13. ^{1}H NMR spectrum of **4c** in tetrachloroethane-d_2 at 130 °C. *Residual solvents.

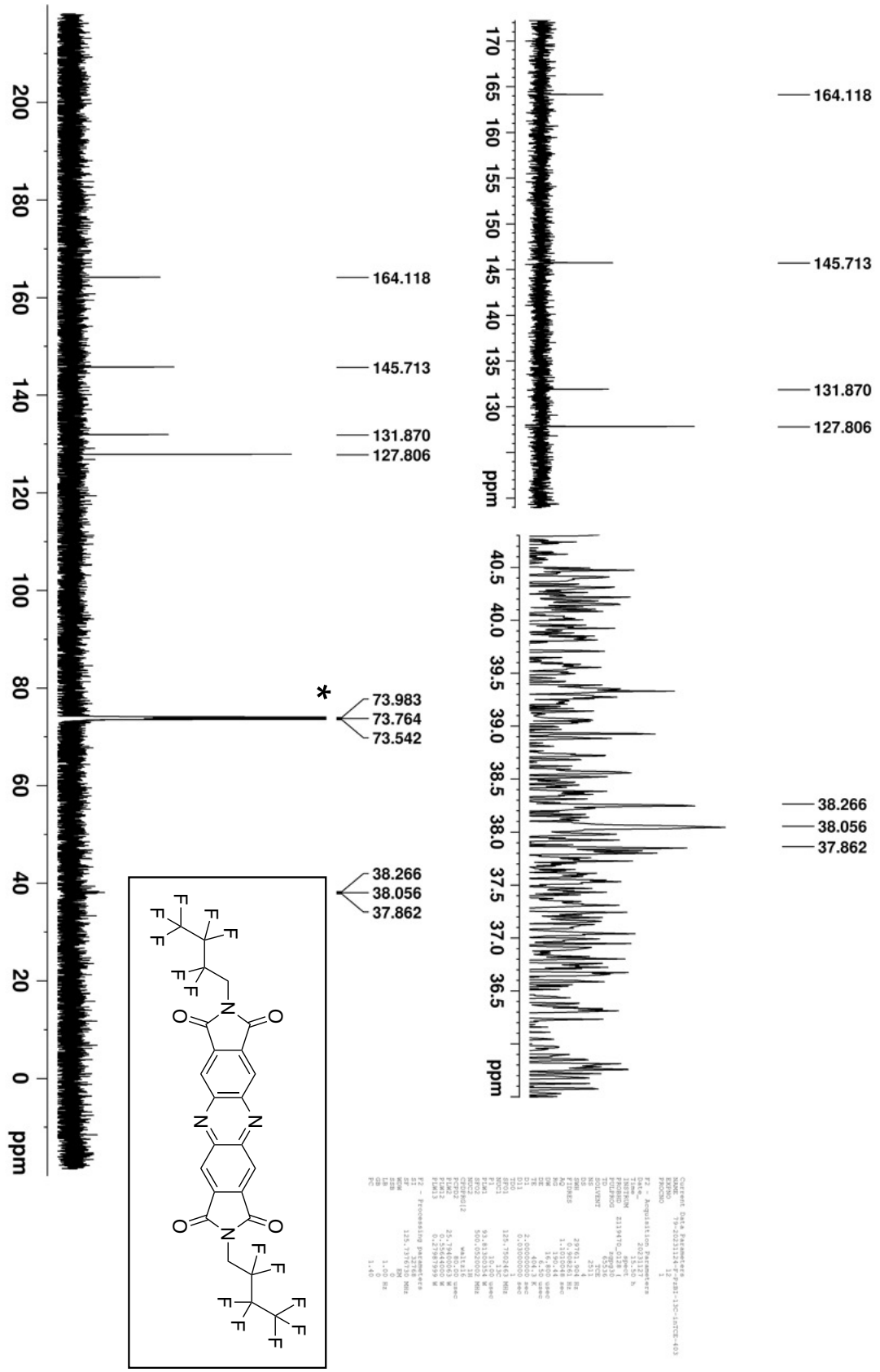

Figure S14. ^{13}C NMR spectrum of **4c** in tetrachloroethane-d_2 at 130 °C. *Residual solvent.

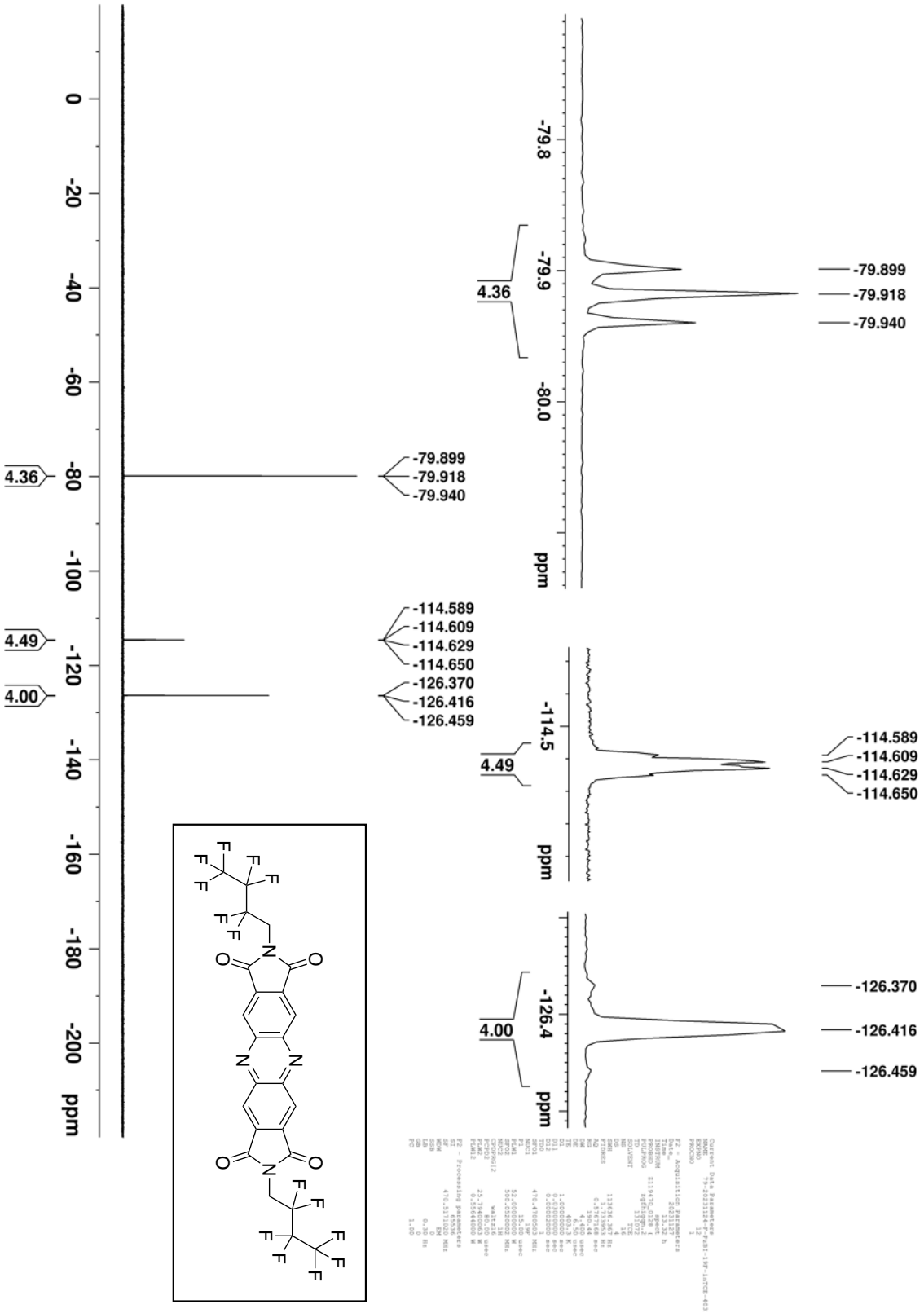

Figure S15. ^{19}F NMR spectrum of **4c** in tetrachloroethane-d_2 at 130 °C.

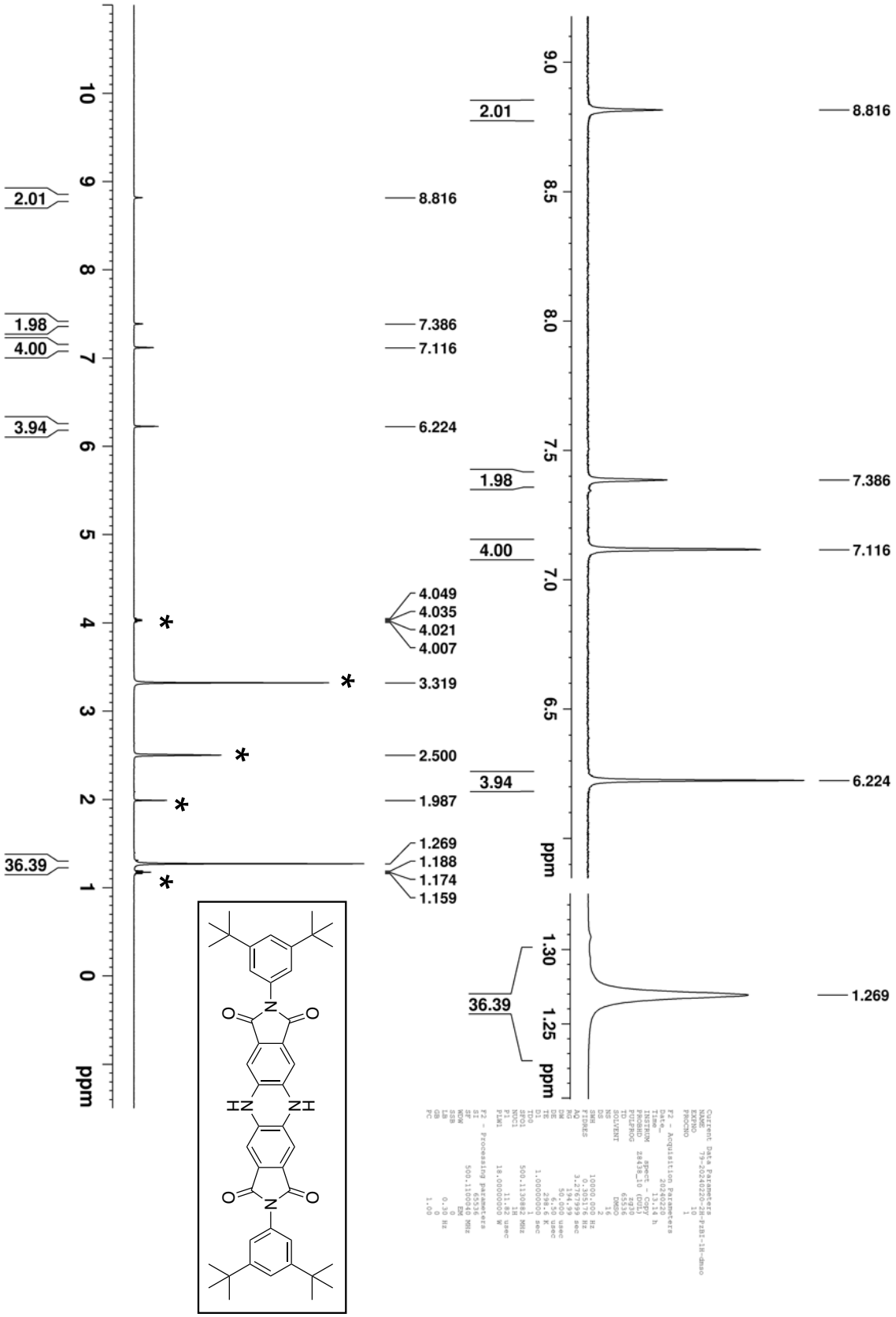

Figure S16. ^{1}H NMR spectrum of **13** in $CDCl_3$ at 25 °C. *Residual DMSO-d_5, AcOEt, and H_2O.

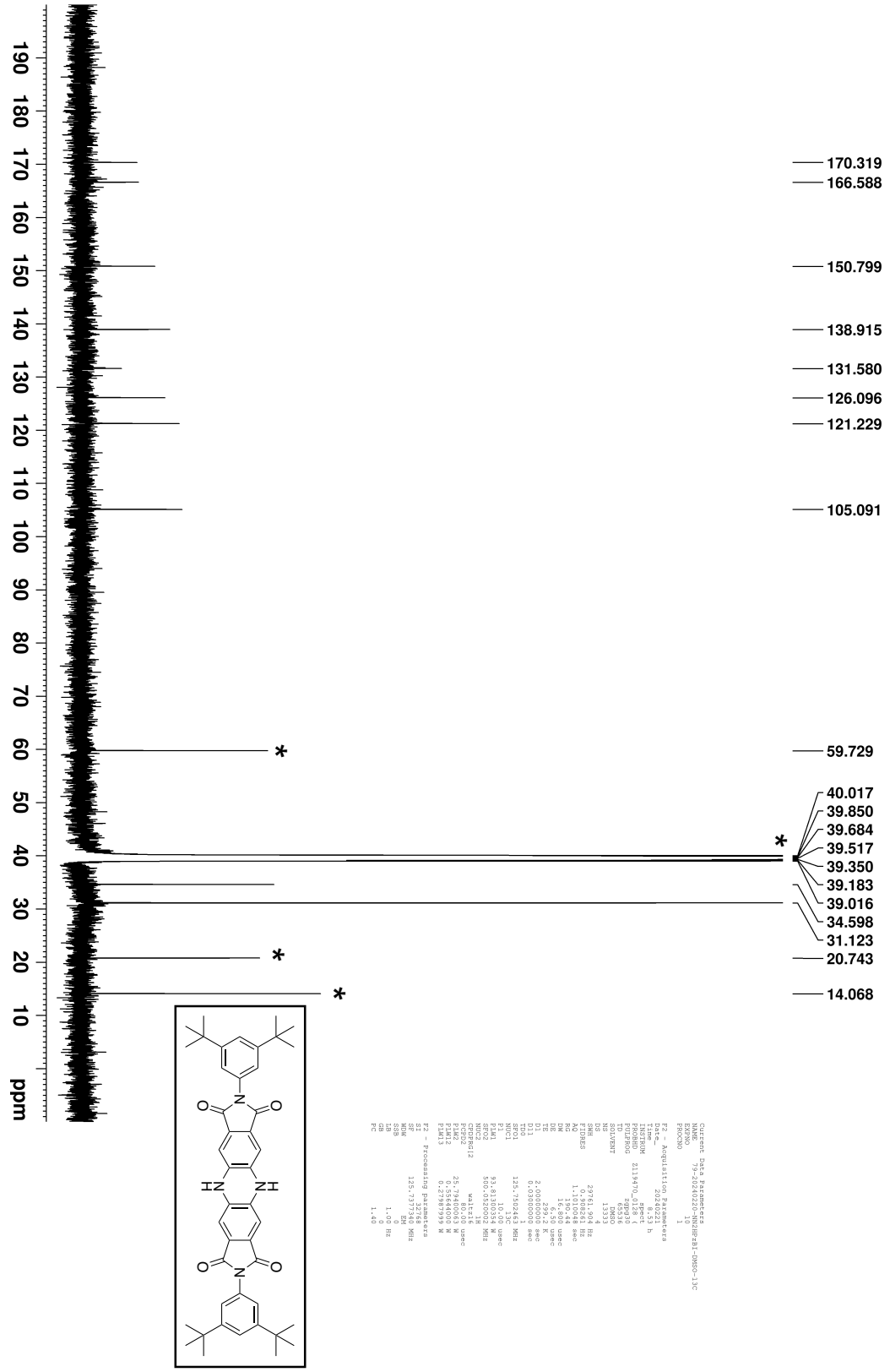

Figure S17. ^{13}C NMR spectrum of **13** in DMSO-d_6 at 25 °C. *Residual AcOEt and DMSO-d_6.

4. Mass spectra

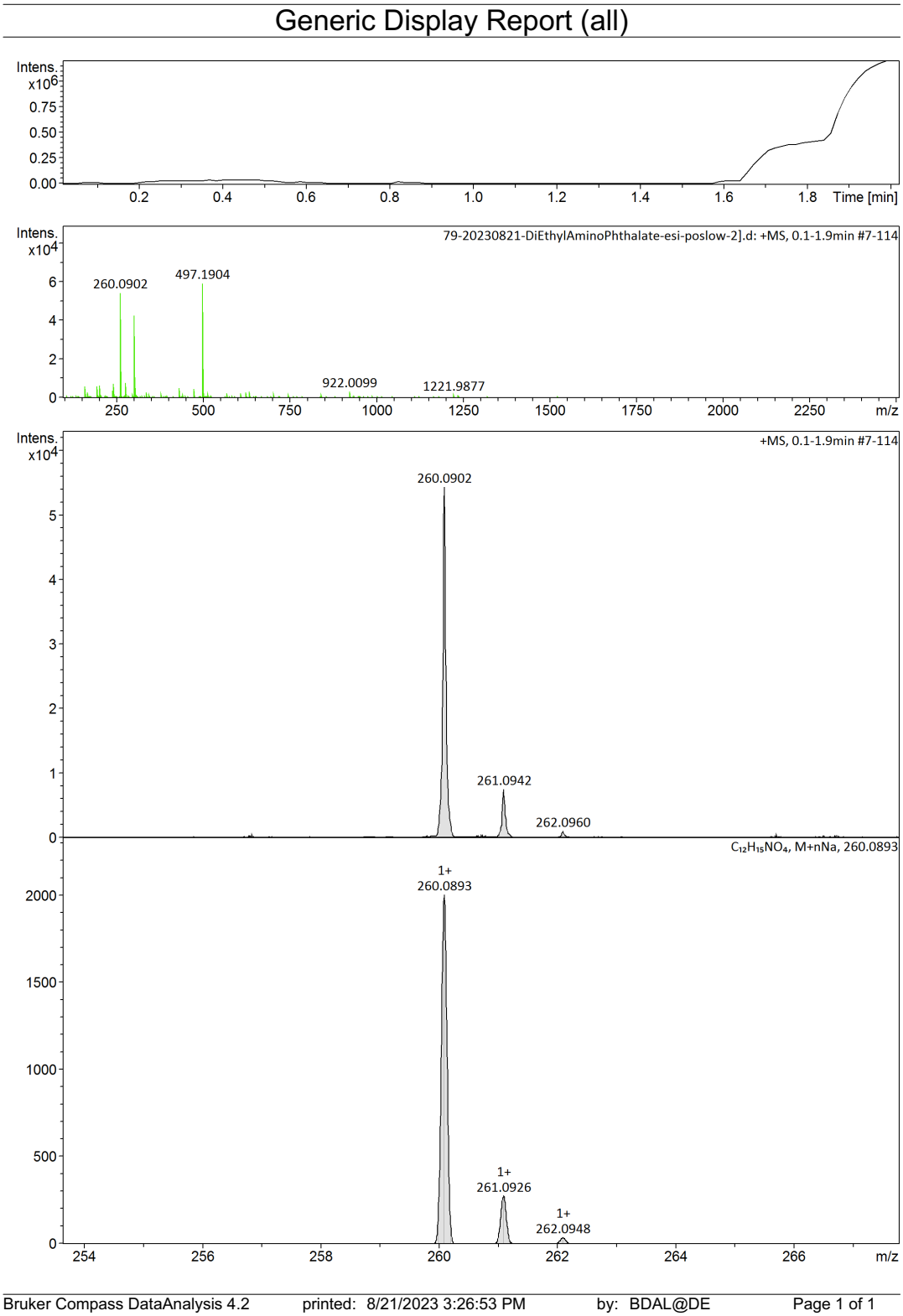

Figure S18. ESI-TOF mass spectrum of **8**.

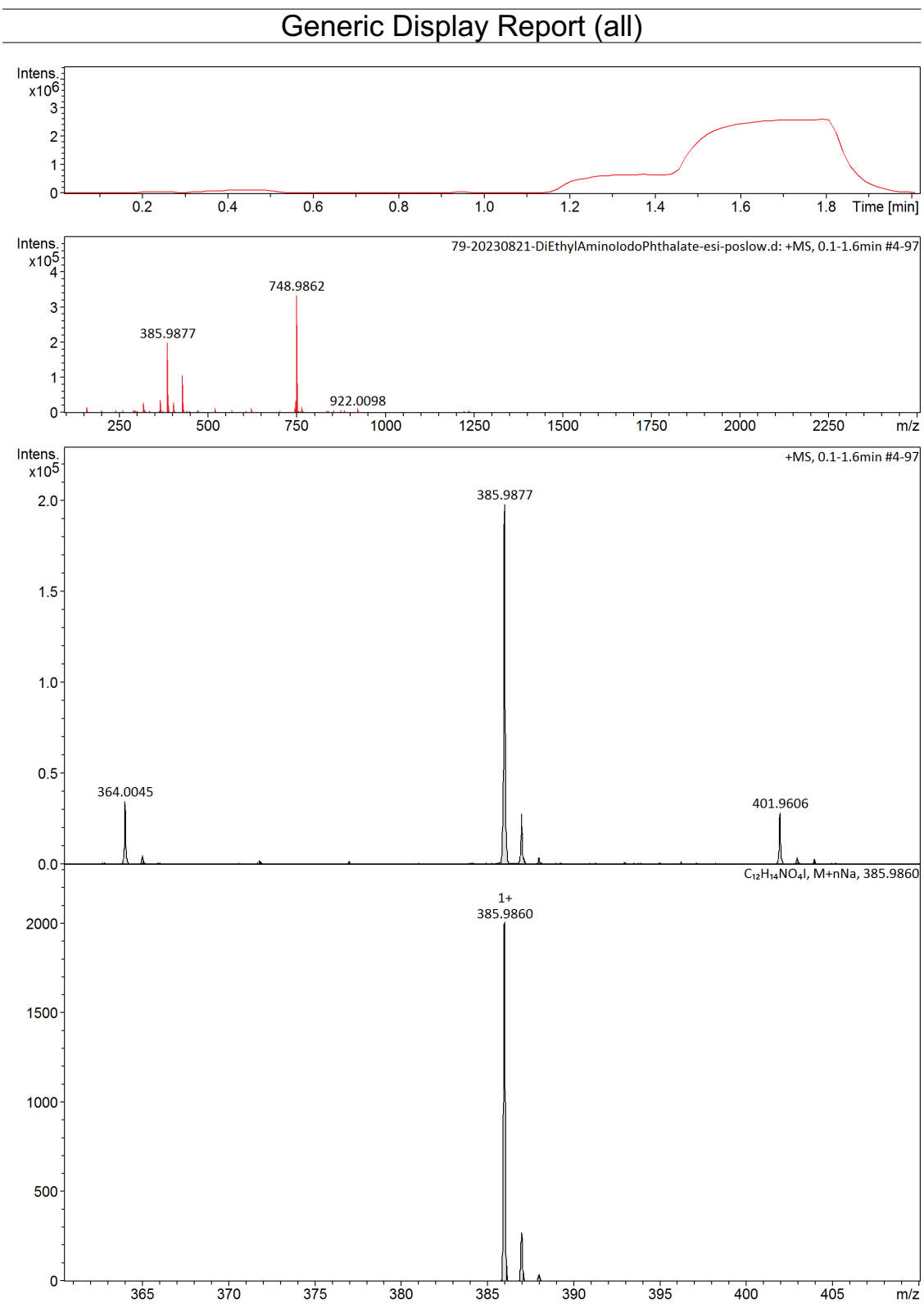

Figure S19. ESI-TOF mass spectrum of **9**.

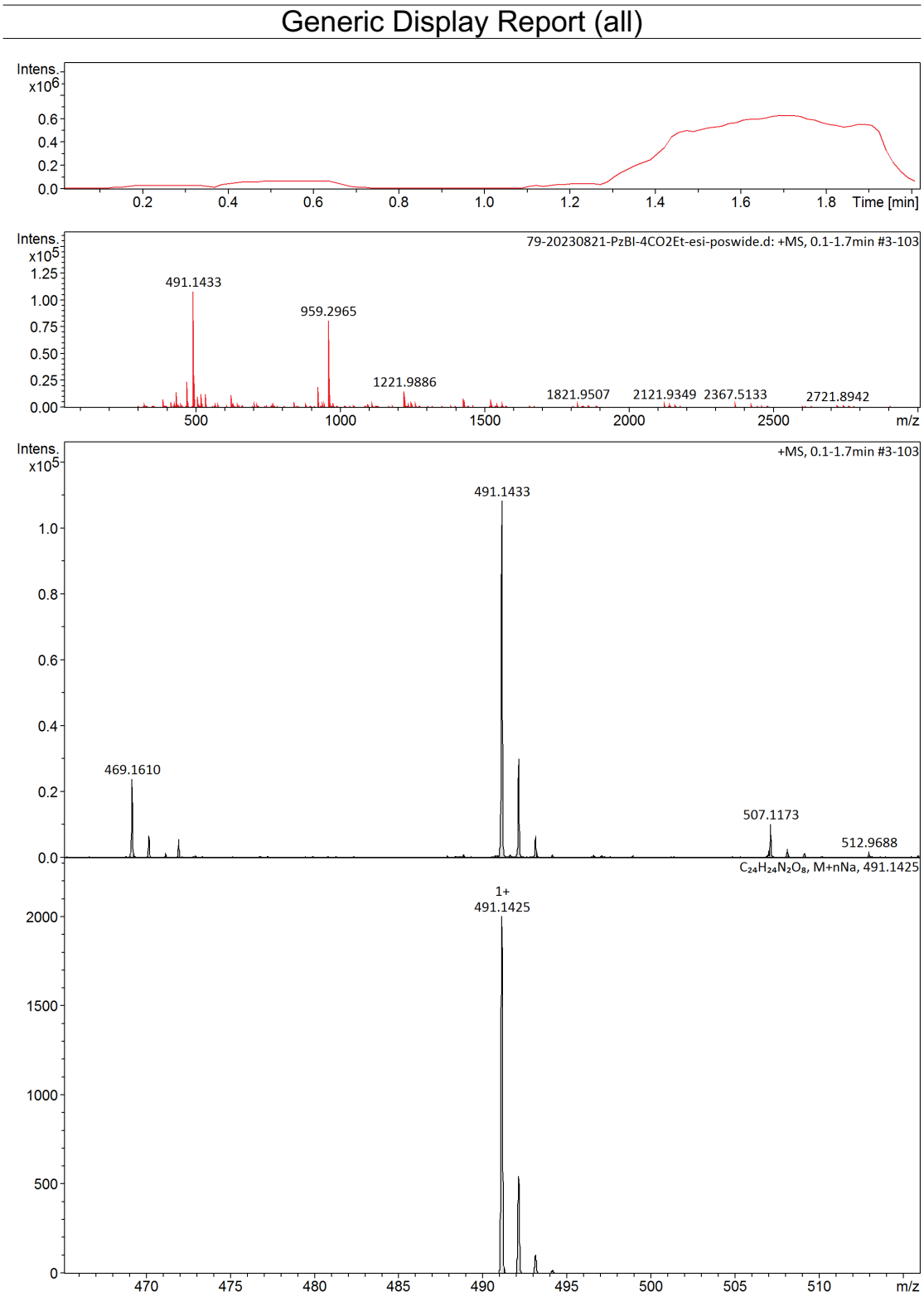

Figure S20. ESI-TOF mass spectrum of **10**.

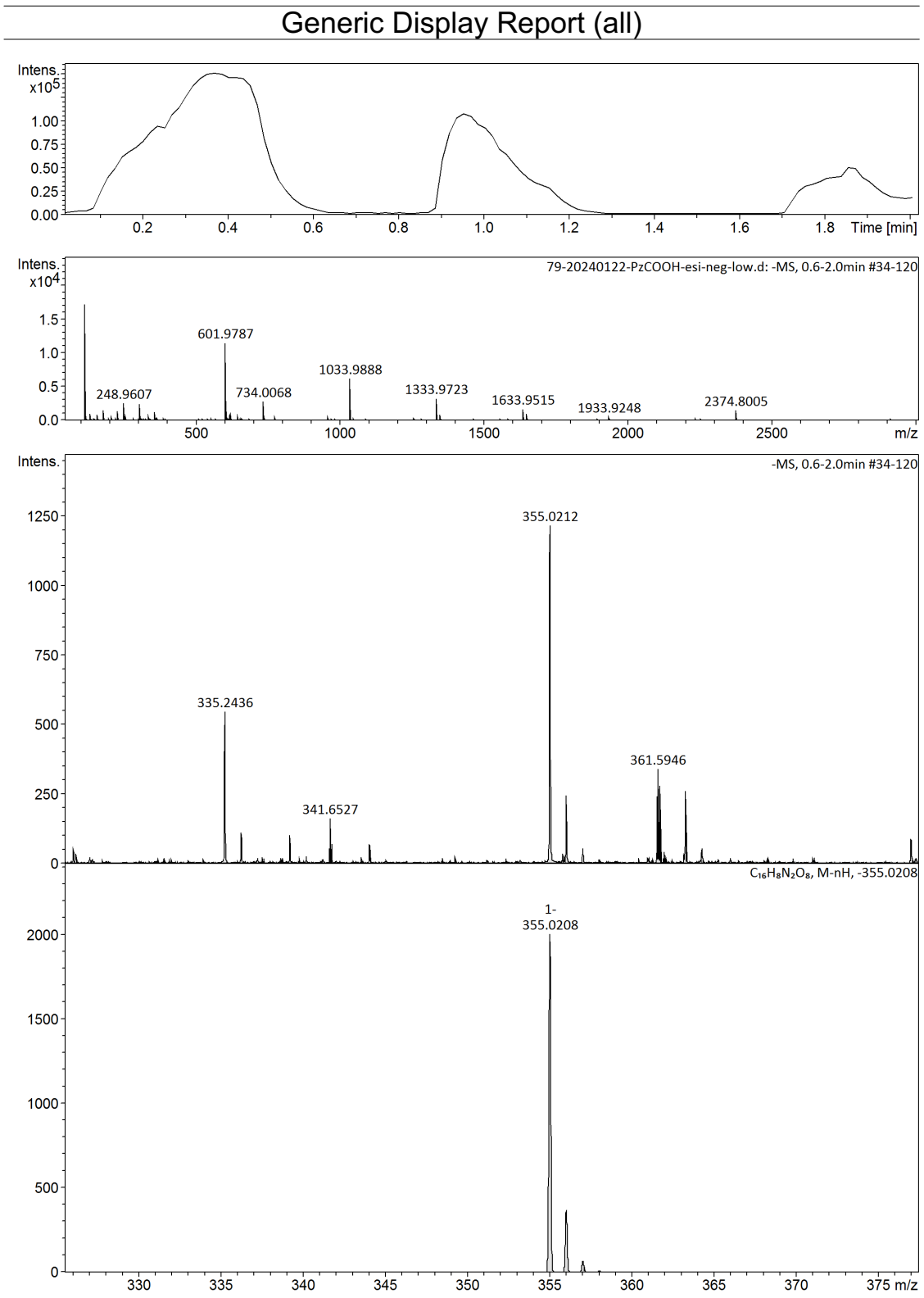

Figure S21. ESI-TOF mass spectrum of **11**.

D:\Data\Shinokubo\tajima\79-20231027-Pz-anhydride-5\0_B10\1\1Lin

Comment 1
Comment 2

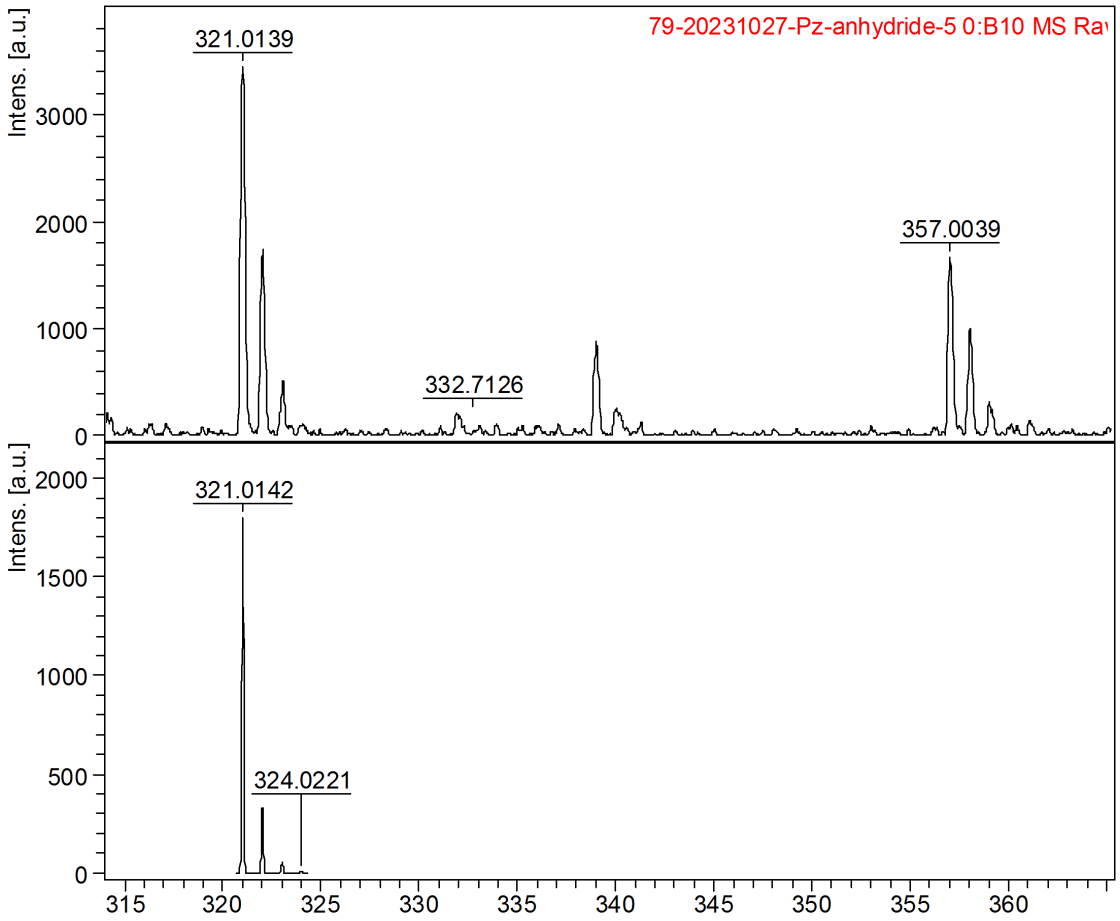

Acquisition Parameter

Date of acquisition	2023-10-27T17:41:39.311+09:00
Acquisition method name	D:\Methods\flexControlMethods\LP_0-2kDa.par
Aquisition operation mode	Linear
Voltage polarity	POS
Number of shots	500
Name of spectrum used for calibration	
Calibration reference list used	APCI-L tuning mix

Instrument Info

User	tof-user
Instrument	FLEX-PC
Instrument type	autoflexTOF/TOF

Bruker Daltonics flexAnalysis printed: 10/27/2023 5:54:21 PM

Figure S22. MALDI-TOF mass spectrum of **12**.

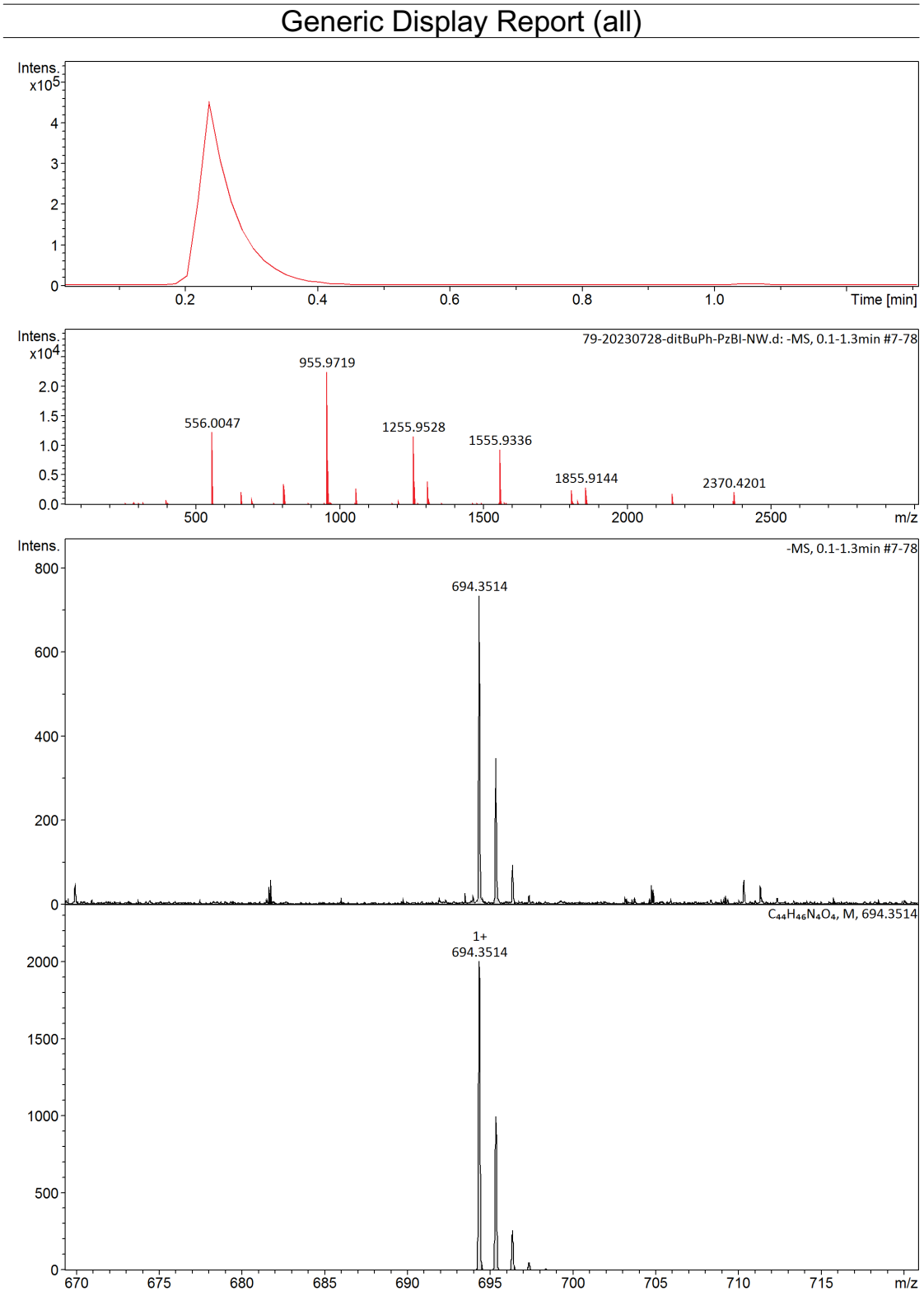

Figure S23. APCI-TOF mass spectrum of **4a**.

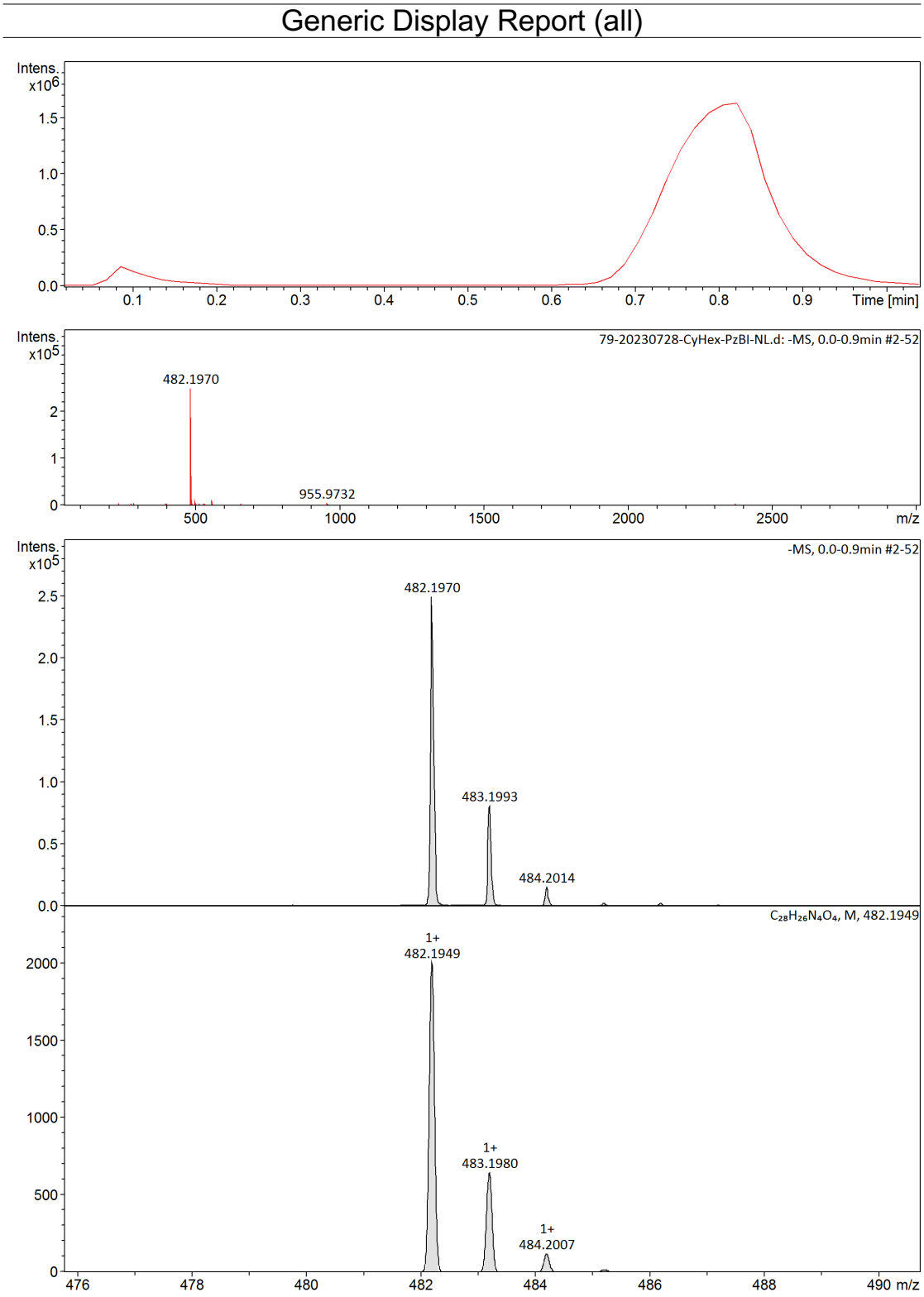

Figure S24. APCI-TOF mass spectrum of **4b**.

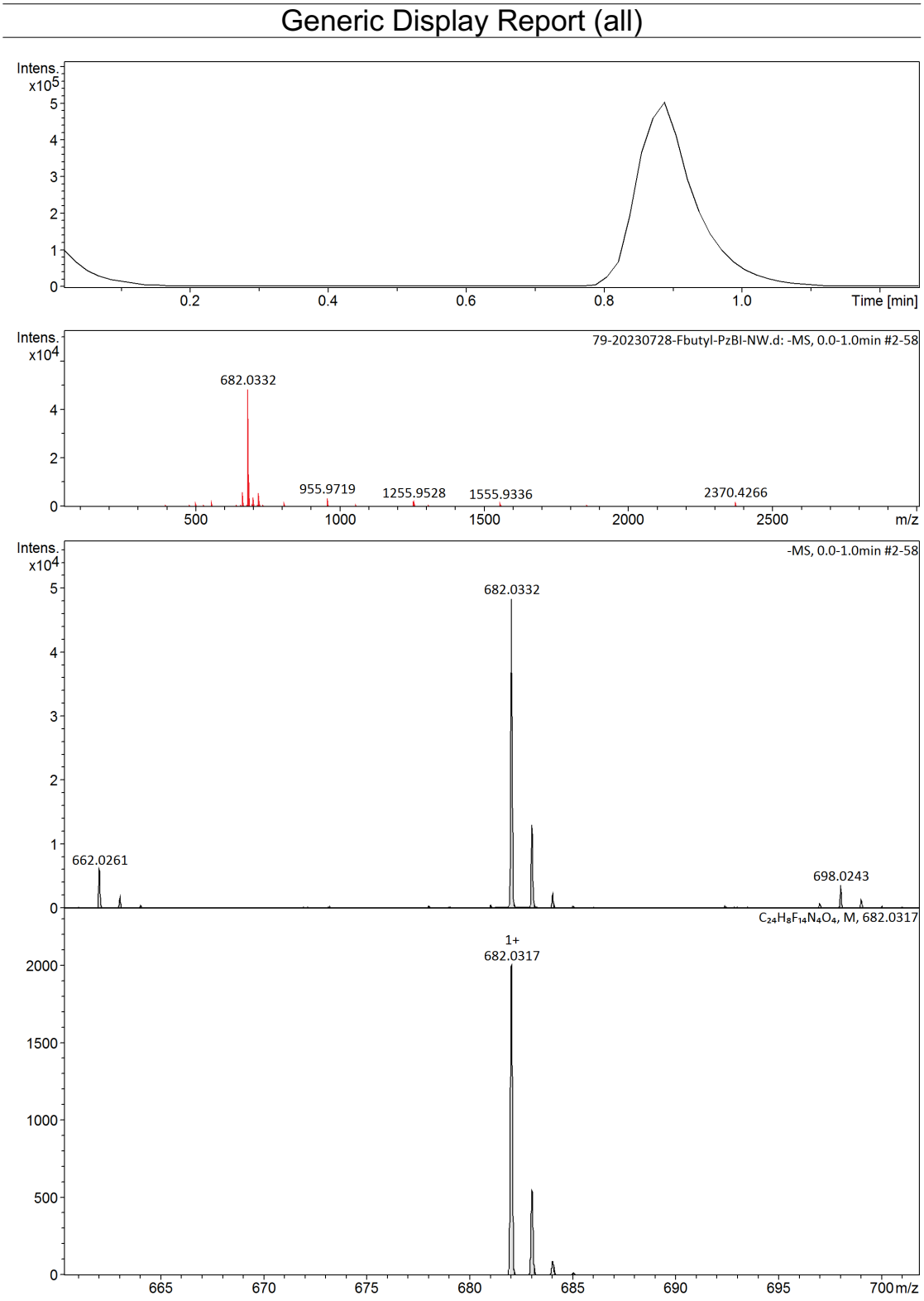

Figure S25. APCI-TOF mass spectrum of **4c**.

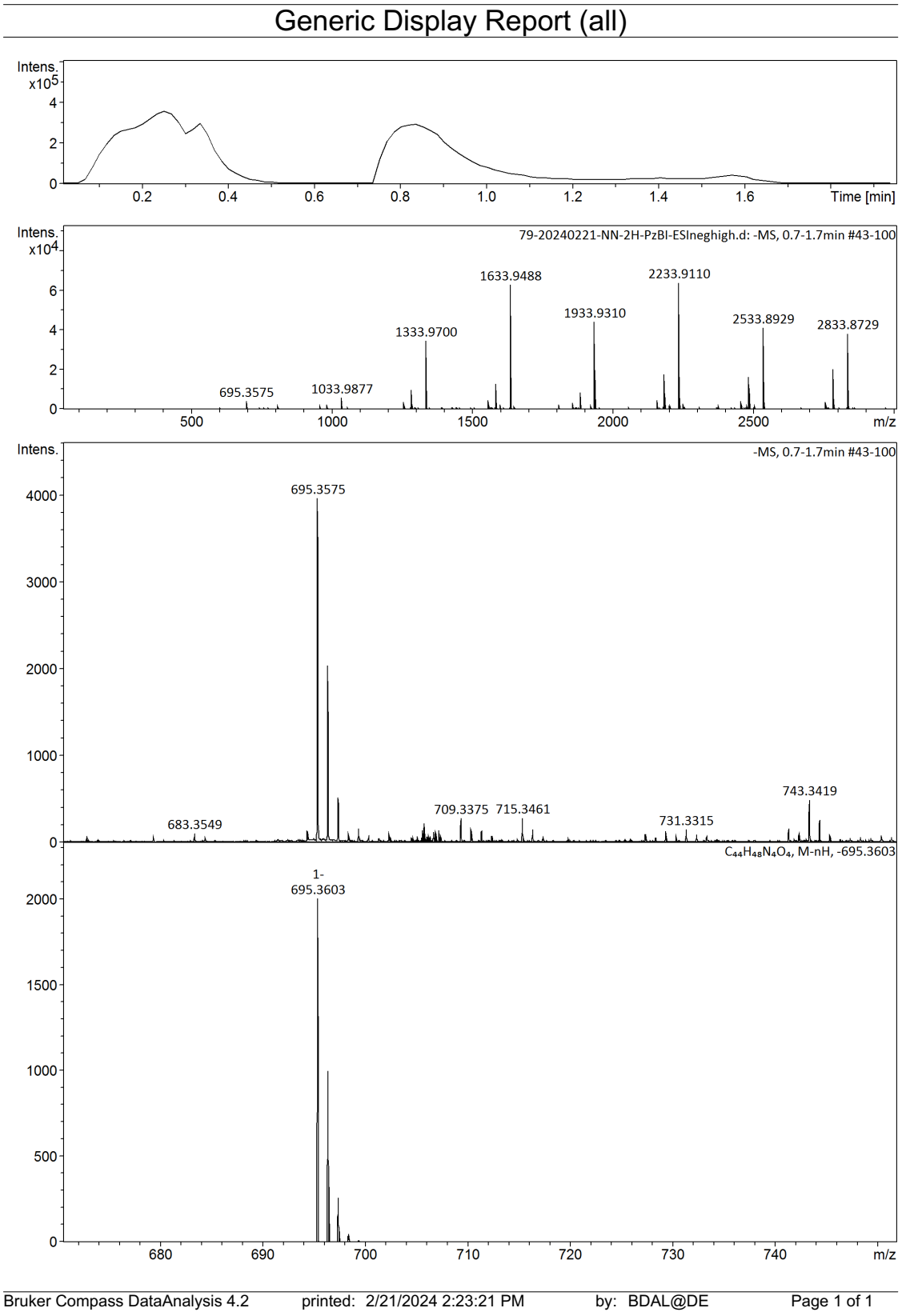

Figure S26. APCI-TOF mass spectrum of **13**.

5. Crystal data

The crystal of **4c** was prepared using the naphthalene flux method.[7] A H shaped glass tube containing **4c** (5 mg) and naphthalene (200 mg) on one side was sealed under vacuum. The sealed glass tube was put in a separable aluminum heating block (Figure S27). One side of the tube containing the sample was heated at 230 °C, and the other side containing naphthalene was heated at 240 °C for 1 h. Then, each part was gradually cooled to 120 °C and 130 °C, respectively, over 12 h. Next, the vacant one was kept at 90 °C for 6 h. After that, the single crystal of **4c** was isolated apart from naphthalene.

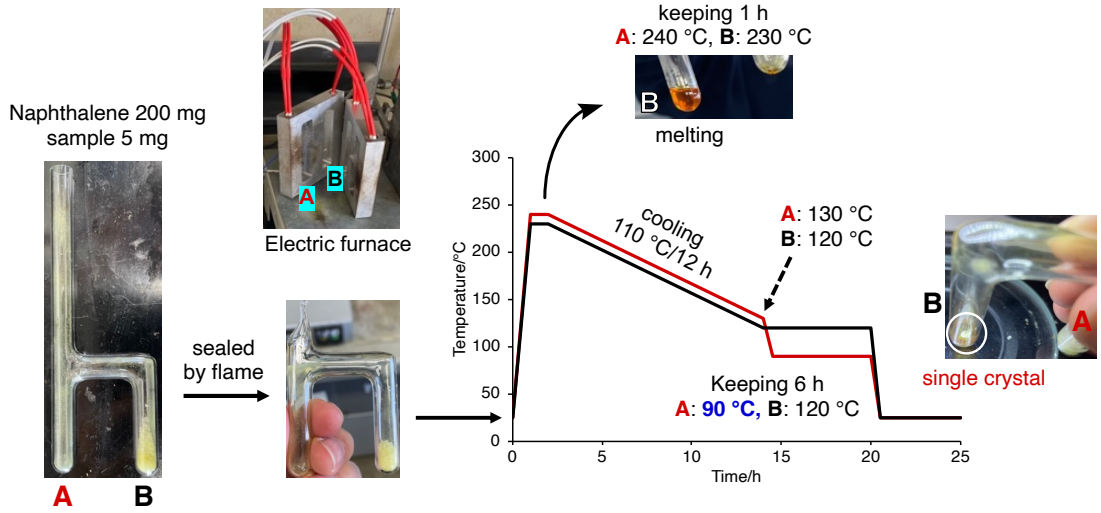

Figure S27. Schematic images and temperature profiles for growth of single crystal of **4c**.

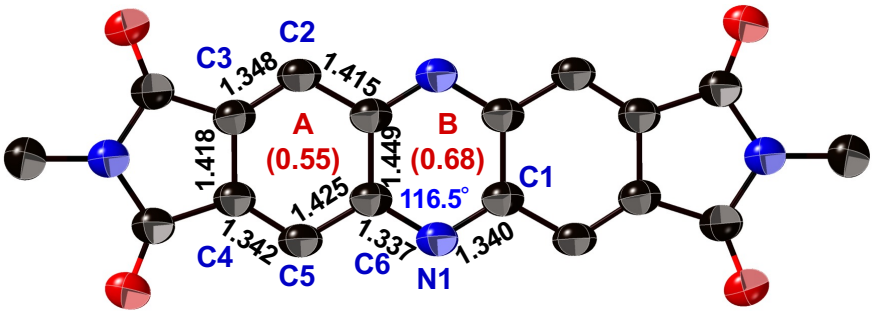

Figure S28. Crystal structure of **4c** with thermal ellipsoids at 50% probability. Hydrogen atoms and substituents on imide groups are omitted for clarity. The value in parentheses shows the HOMA value.

Table S1. Crystallographic data of **4b**, **4c**, and **6**.

compound	**4b**	**4c**	**6**
formula	$C_{28}H_{26}N_4O_4$	$C_{24}H_8F_{14}N_4O_4$	$C_{30}H_{28}N_2O_4$
formula weight	482.53	682.34	480.54
crystal system	triclinic	triclinic	monoclinic
space group	*P*–1 (#2)	*P*–1 (#2)	*I*2/*a* (#15)
crystal color	yellow	yellow	colorless
crystal description	plate	plate	needle
a [Å]	5.1483(2)	5.2387(3)	22.6197(11)
b [Å]	6.1694(2)	5.8596(4)	5.2092(2)
c [Å]	18.5347(6)	21.0219(14)	38.7744(17)
a [°]	86.250(3)	92.930(5)	–
b [°]	82.260(3)	94.979(5)	91.172(4)
γ [°]	81.884(3)	96.674(5)	–
V [Å^3]	576.85(4)	637.29(7)	4567.9(3)
Z	1	1	8
d_{calcd} [g cm^{-3}]	1.389	1.778	1.398
R_1 ($I > 2s(I)$)	0.0506	0.0808	0.0888
wR_2 (all data)	0.1749	0.2935	0.2334
GOF	1.038	1.061	1.030
Temperature [K]	293(2)	293(2)	93(2)
solvent	*o*-$C_6H_4Cl_2$/ octane	naphthalene flux	toluene
CCDC	2348427	2348428	2348426

6. Electron-transporting behavior

For fabricating thin-film OFETs, the substrates modified with self-assembled monolayers (SAMs) of 12-cyclohexyldodecylphosphonic acid (CDPA) were used. SAM-modified substrates were prepared as described in the literature.[8] Heavily n-doped Si wafers with a 300 nm-thick thermally grown SiO_2 layer were used as substrates. The Si/SiO_2 substrates were cleaned with deionized water, acetone, and 2-propanol for 10 min in an ultrasonic bath. Substrates were dried with a flow of N_2 gas and then treated by UV–O_3 cleaner (Filgen UV253V8) for 45 min. A solution of $Al(NO_3)_3 \cdot 9H_2O$ in ethanol (0.1 M) was spin-coated (5000 rpm, 40 s) on cleaned substrates in an N_2 glove box, and the substrates were annealed at 300 °C for 30 min in air to form Al_2O_3 layer. The Al_2O_3-coated substrates were treated with UV–O_3 cleaner for 45 min and then soaked in a solution of CDPA in 2-propanol (1.5 mM) at room temperature for 12 h. Finally, substrates were washed with 2-propanol and deionized water and then dried with a flow of N_2 gas to afford SAM-modified substrates. The average capacitance per unit area of the dielectric layer (C_i) of the insulating layer prepared by this method was measured to be 10 nF cm^{-2}.[9] The active layer was prepared by vacuum-deposition method using solid of **4b** and **4c** for 500 Å at 0.3–0.8 Å s^{-1} under the pressure of ~5×10^{-4} Pa. The top contact source and drain electrodes of gold films (thickness = 300 Å) were vacuum deposited under the pressure of ~5×10^{-4} Pa through a shadow mask on the active layer (Figure S29). The drain–source channel length (L) and width (W) was 50 μm and 1000 μm, respectively. The gold electrodes were deposited in the same manner as the thin-film OFETs. The L and W values were measured to be 60.0 μm and 69.4 μm, respectively, using a Zeiss Axio Scope A1 optical microscope. The output and transfer characteristics of the OFETs were measured using a vacuum prober system (Thermal Block Company, SB-MCPS-NAT) and a Keithley 2400 semiconductor characterization system under vacuum at the pressure of ~3×10^{-1} Pa and atmospheric conditions. The field-effect mobilities (μ) of the OFETs were determined from the forward transfer curve in the saturation regime (V_{DS} = 80 V for **4b** and V_{DS} = 60 V for **4c**) and regime (V_{DS} = 5V) using the following equation,

$$I_{DS} = \mu W C_i (V_G - V_{th})^2 / 2L \text{ (saturation regime)}$$

$$I_{DS} = \mu W C_i V_{DS} \{2(V_G - V_{th}) - V_{DS}\} / 2L \text{ (linear regime)}$$

Where I_{DS} is the drain–source current and V_{DS}, V_G, and V_{th} are the drain–source voltage, gate voltage, and threshold voltage, respectively. The on/off ratios (I_{on}/I_{off}) were determined from the I_{DS} at V_G = 0 V (I_{off}) and V_G = 80 V (I_{on}). The averaged μ values ($\mu_{average}$) of the thin-film OFETs were calculated from nine devices for **4b** and seventeen devices for **4c**.

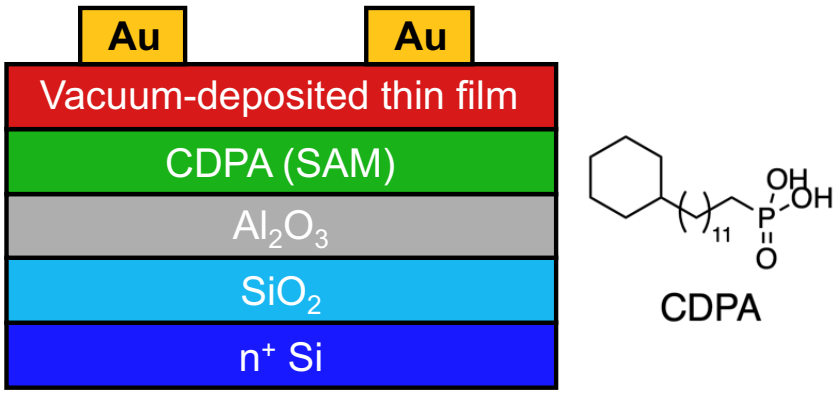

Figure S29. Schematic description of the thin-film OFET device composition.

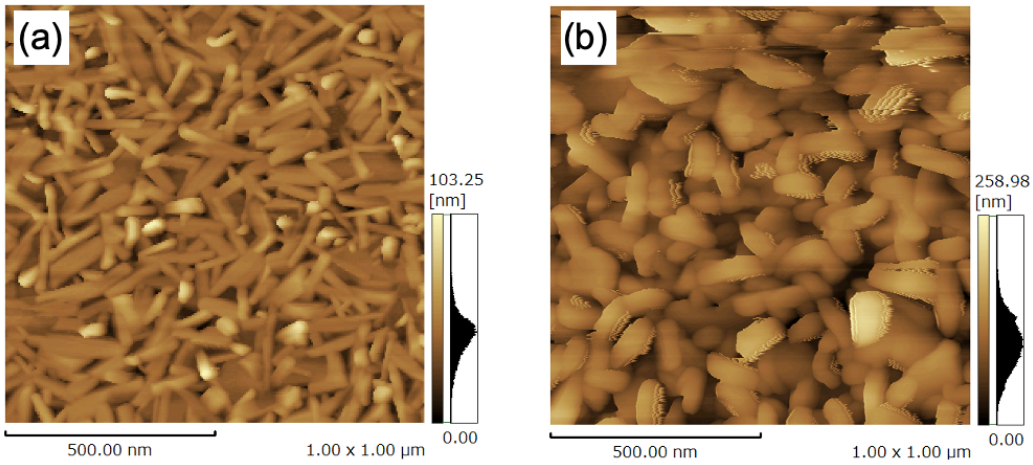

Figure S30. AFM images of vacuum-deposited films of **4b** and **4c**.

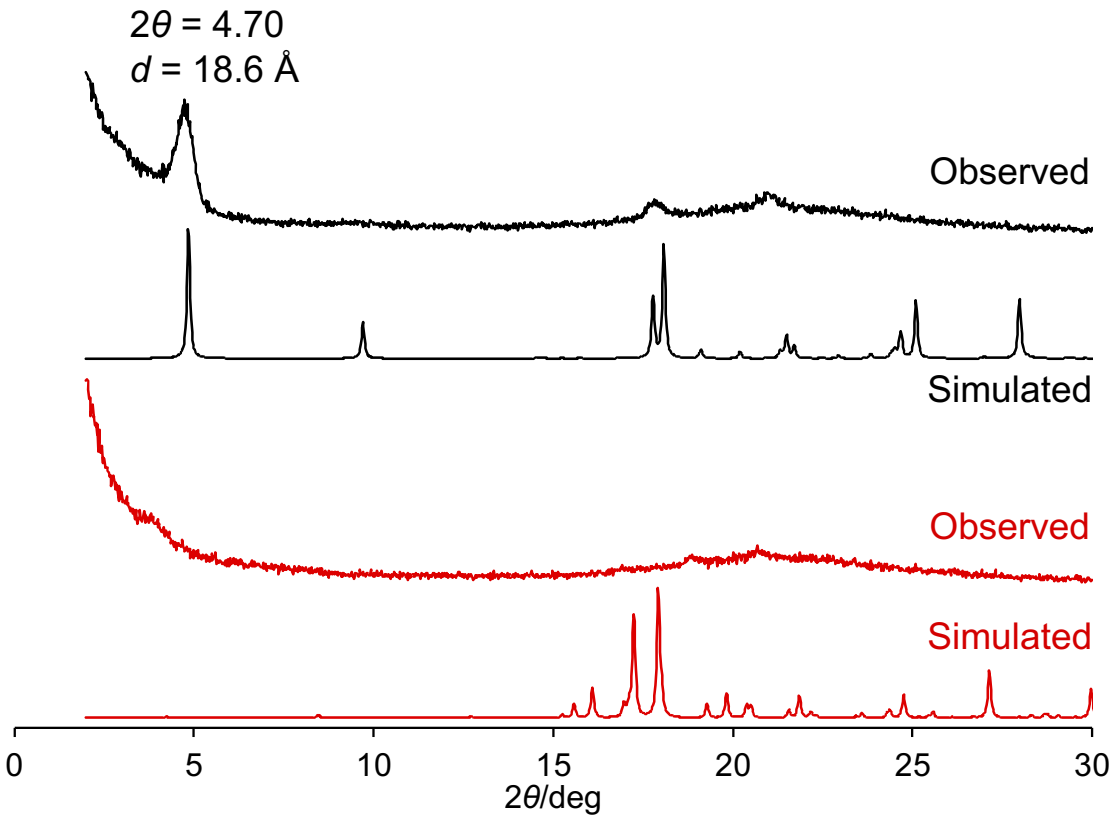

Figure S31. Thin film out-of-plane X-ray diffraction patterns of vacuum-deposited film of **4b** (black line) and **4c** (red line). Upper lines are observed patterns. Lower lines are simulated patterns from the single crystal structure.

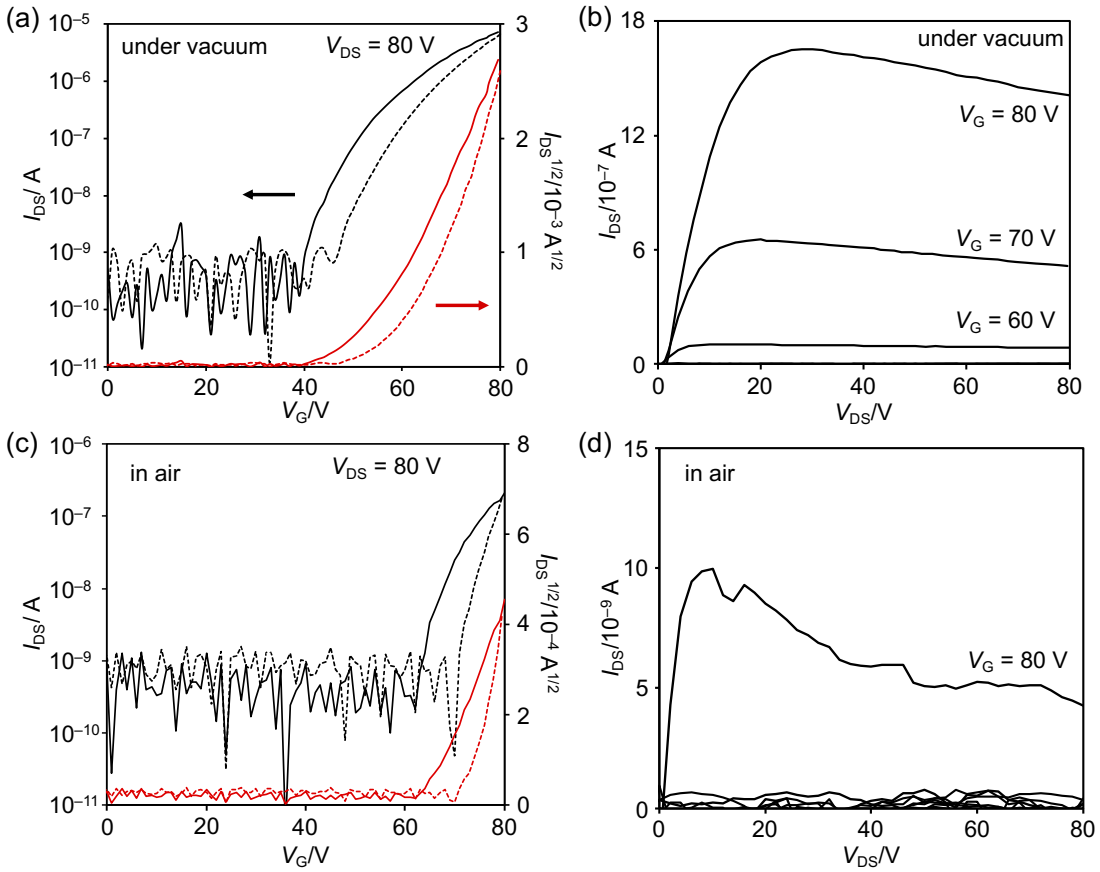

Figure S32. Thin-film OFET properties of **4b** under (a,b) vacuum and (c,d) ambient conditions. (a,c) Transfer characteristics. (b,d) Output characteristics.

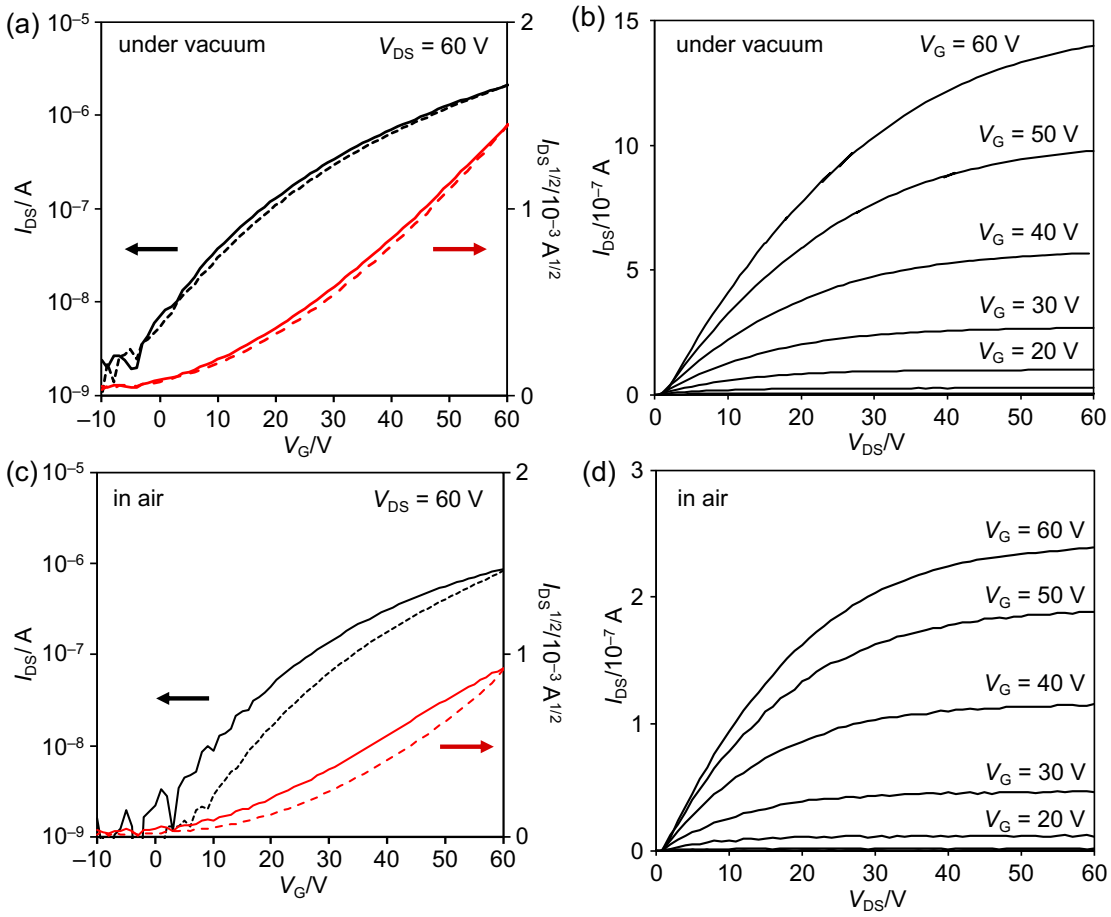

Figure S33. Thin-film OFET properties of **4c** under (a,b) vacuum and (c,d) ambient conditions. (a,c) Transfer characteristics. (b,d) Output characteristics.

Table S2. Vacuum-deposited OFET characteristics in saturated region of **5b** and **5c**.

	condition	μ_{max} [$cm^2\ V^{-1}\ s^{-1}$]	$\mu_{average}$ [$cm^2\ V^{-1}\ s^{-1}$]	V_{th} [V]	I_{on}/I_{off} [-]
4b	vacuum	9.9×10^{-2}	$(4.6 \pm 2.4) \times 10^{-2}$	46 ± 13	$(3.4 \pm 7.8) \times 10^{6}$
	air	6.4×10^{-3}	$(2.2 \pm 0.8) \times 10^{-2}$	61 ± 4	$(2.7 \pm 2.6) \times 10^{4}$
4c	vacuum	8.2×10^{-3}	$(5.7 \pm 2.9) \times 10^{-3}$	11 ± 3	$(3.5 \pm 2.5) \times 10^{3}$
	air	3.5×10^{-3}	$(2.6 \pm 1.7) \times 10^{-3}$	7.3 ± 5.2	$(1.3 \pm 1.2) \times 10^{3}$

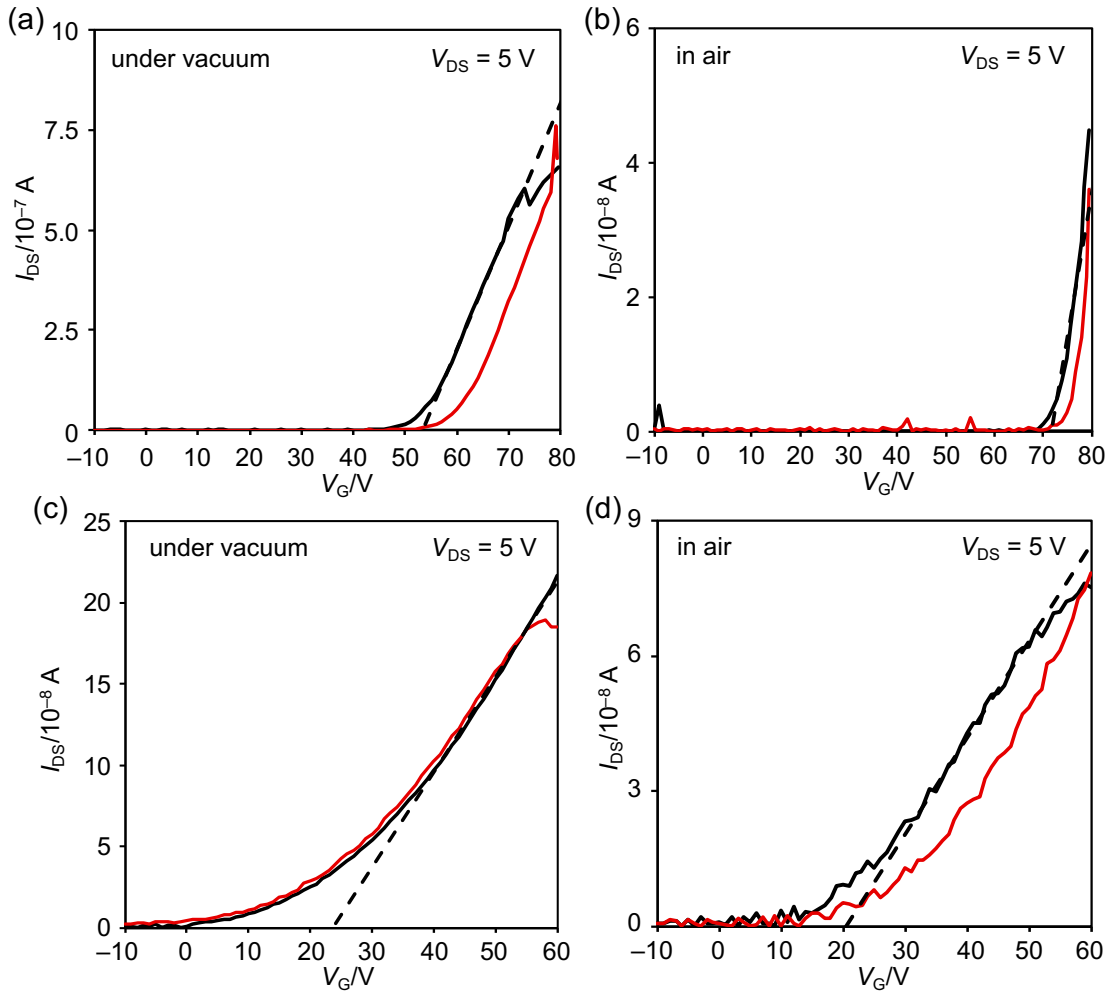

Figure S34. Transfer characteristics in the linear regime of thin-film OFET properties of (a,b) **4b** and (c,d) **4c** under (a,c) vacuum and (b,d) ambient conditions. Black line: forward sweeping. Red line: backward sweeping.

Table S3. Vacuum-deposited OFET characteristics in linear region of **4b** and **4c**.

	condition	μ_{max} [$cm^2\ V^{-1}\ s^{-1}$]	$\mu_{average}$ [$cm^2\ V^{-1}\ s^{-1}$]	V_{th} [V]	I_{on}/I_{off} [-]
4b	vacuum	3.1×10^{-2}	$(2.4 \pm 0.5) \times 10^{-2}$	53± 8	$(6.8 \pm 8.4) \times 10^4$
	air	5.9×10^{-3}	$(4.1 \pm 1.7) \times 10^{-3}$	18 ± 4	$(3.1 \pm 6.4) \times 10^3$
4c	vacuum	4.3×10^{-2}	$(2.2 \pm 0.5) \times 10^{-3}$	64 ± 8	$(3.3 \pm 7.2 \times 10^5$
	air	2.1×10^{-3}	$(1.4 \pm 0.4) \times 10^{-3}$	22 ± 3	$(1.1 \pm 2.8) \times 10^4$

7. TRMC measurement

Transient photoconductivity was measured by an FP-TRMC setup. A resonant cavity with Q ~ 2500 was used to obtain a high degree of sensitivity in the conductivity measurement. Proving microwave frequency and power were set at ~9.1 GHz and 3.0 mW, respectively, such that the electric field of the microwave was sufficiently small not to disturb the translational motion of charge carriers. The observed value of photoconductivity converted to the product of the quantum yield φ and the sum of charge-carrier mobilities $\Sigma\mu$ by $\varphi\Sigma\mu = \Delta\sigma\ (eI_0F_{\text{light}})^{-1}$, where e, I_0, Flight and $\Delta\sigma$ are the unit charge of a single electron, incident photon density of excitation laser (photons per m^2), a correction factor (m^{-1}) and transient photoconductivity, respectively. The sample was set at the point of the electric field maximum in a resonant cavity. FP-TRMC experiments were performed at room temperature under O_2 or argon-saturated conditions by continuous flowing for over 10 min. The measurements of all the samples were performed for polycrystalline samples. These samples were fixed on a quartz substrate by poly(vinyl alcohol) binders.

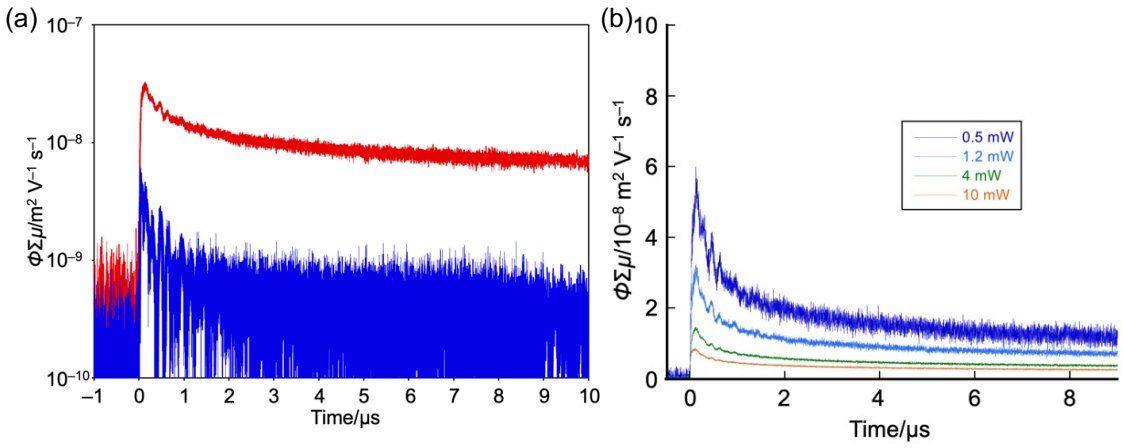

Figure S35. (a) Conductivity transients in **4b** (blue line) and **4c** (red line) observed by FP-TRMC spectroscopy upon excitation at 355 nm laser pulses at 1.8 × 10^{15} photons cm^{-2}. (b) Conductivity transient observed in **4c** upon modulated excitation density at 355 nm from 4.5 × 10^{14}–9.1 × 10^{15} photons cm^{-2}.

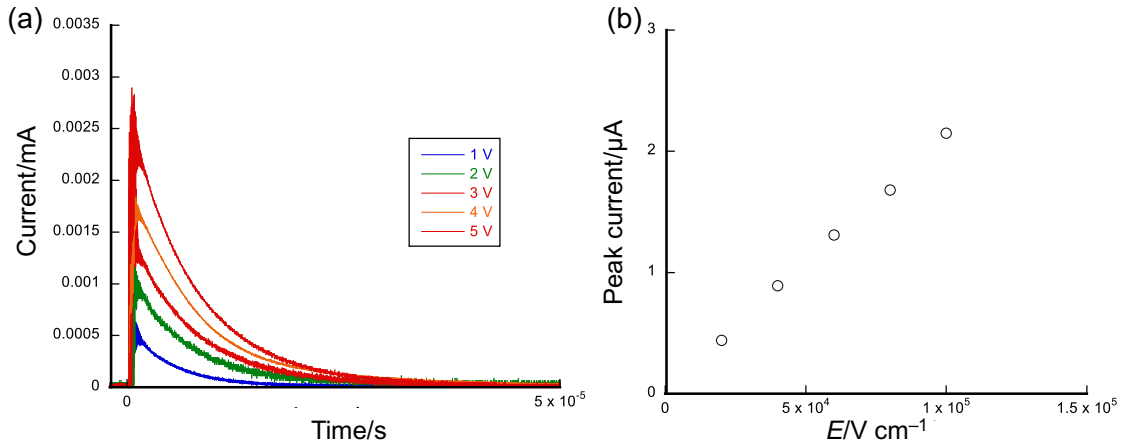

Figure S36. (a) Photocurrent transient observed in pristine thin film of **4c** cast onto electrodes with 5 μm gap upon excitation at 355 nm laser pulses at 4.1×10^{15} photons cm^{-2}. (b) Dependence on observed photocurrent on bias applied to the gap at $E = 2.0 \times 10^4$–10×10^4 V cm^{-1}.

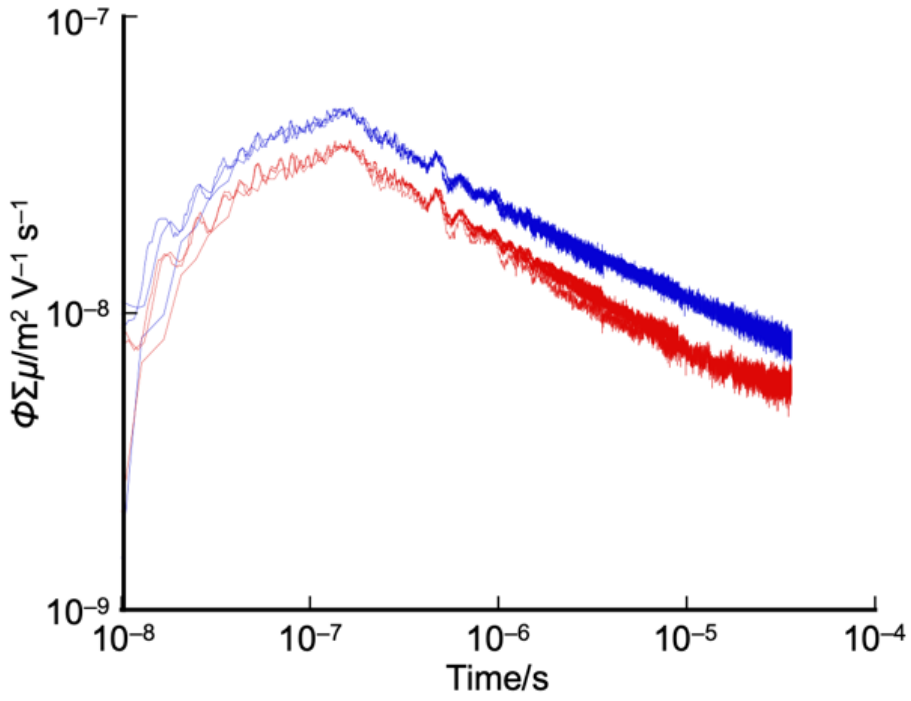

Figure S37. Global kinetic traces of transient photoconductivity observed for **4c** in air or SF_6 upon excitation at 355 nm laser pulses at 4.1×10^{15} photons cm^{-2}.

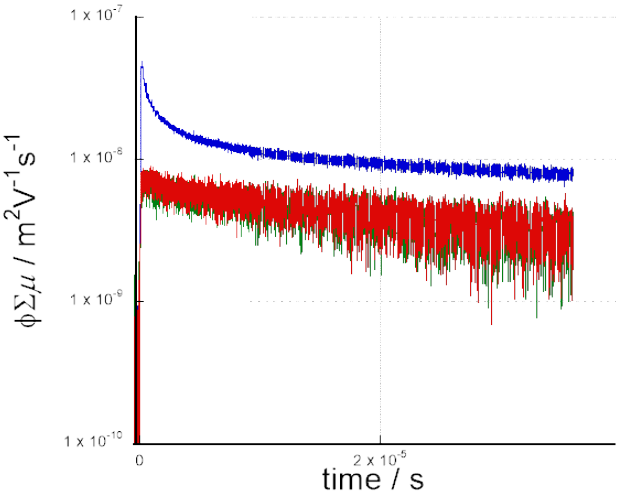

Figure S38. Conductivity transients in **4b** (blue line) and **6** (red and green lines, green: reproducibility checking under identical conditions) observed by FP-TRMC spectroscopy upon excitation at 355 nm laser pulses at 1.8×10^{15} photons cm^{-2}.

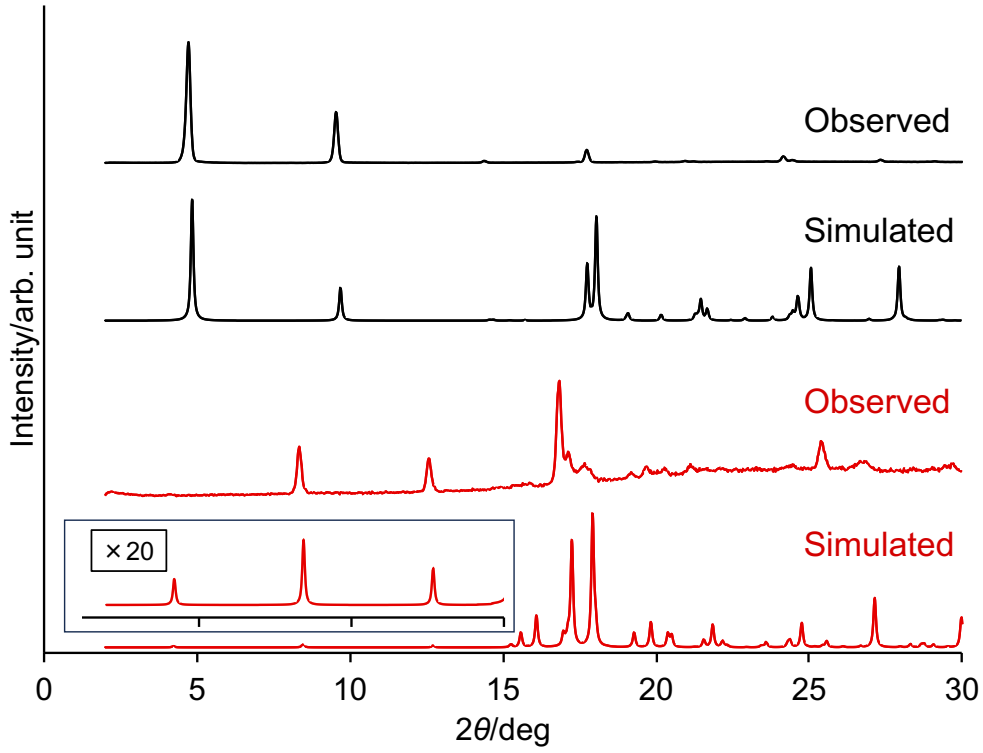

Figure S39. Powder X-ray diffraction patterns of crystalline powder samples of **4b** (black line) and **4c** (red line). Upper lines are observed patterns. Lower lines are simulated patterns from the single crystal structure. The inset shows an enlarged simulated pattern of **4c**.

8. DFT calculations

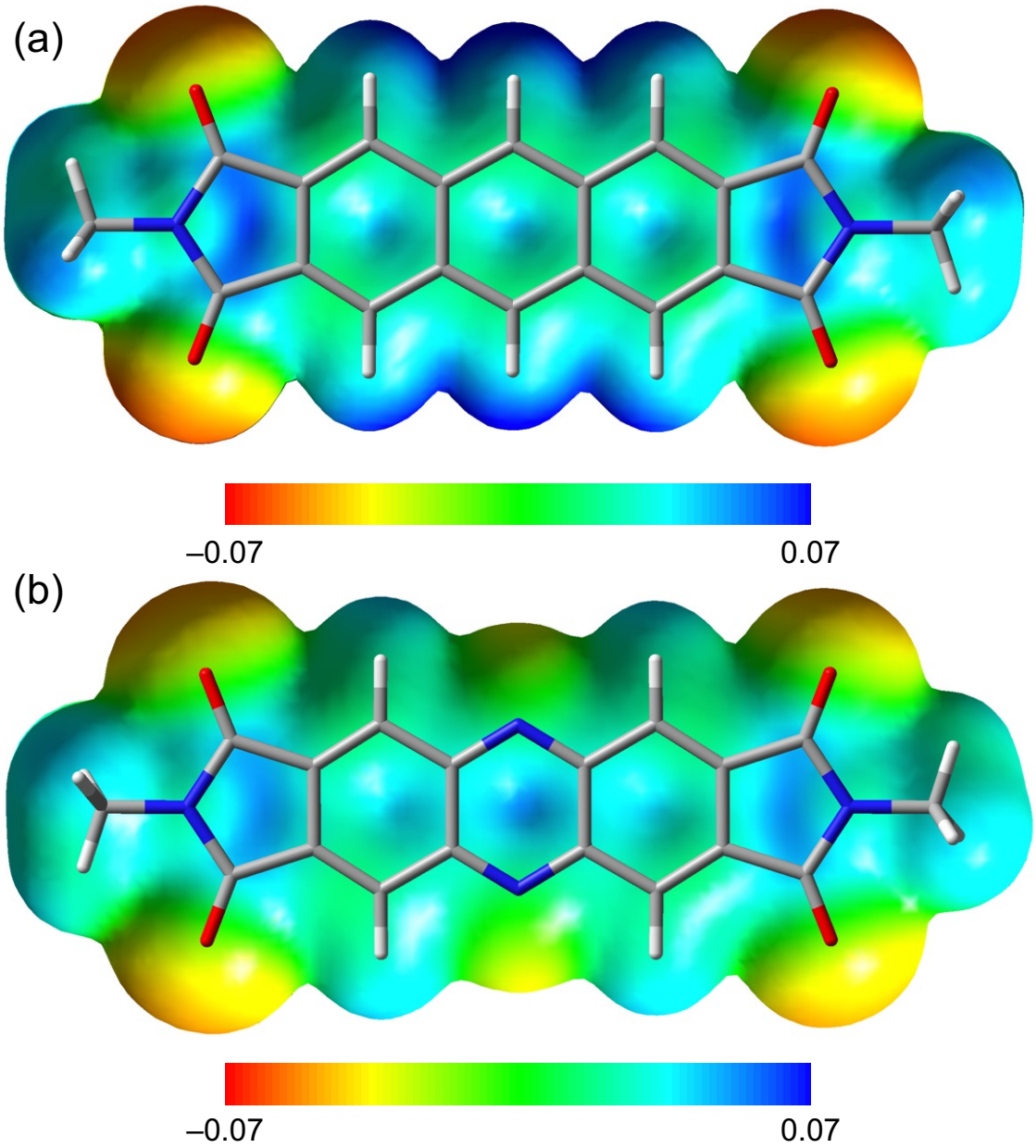

Figure S40. Electron static potential maps of (a) **6** and (b) **4**. DFT calculations were conducted at the B3LYP/6-31G+(d,p) level. The substituents on the imide groups are replaced with methyl groups to simplify the calculations.

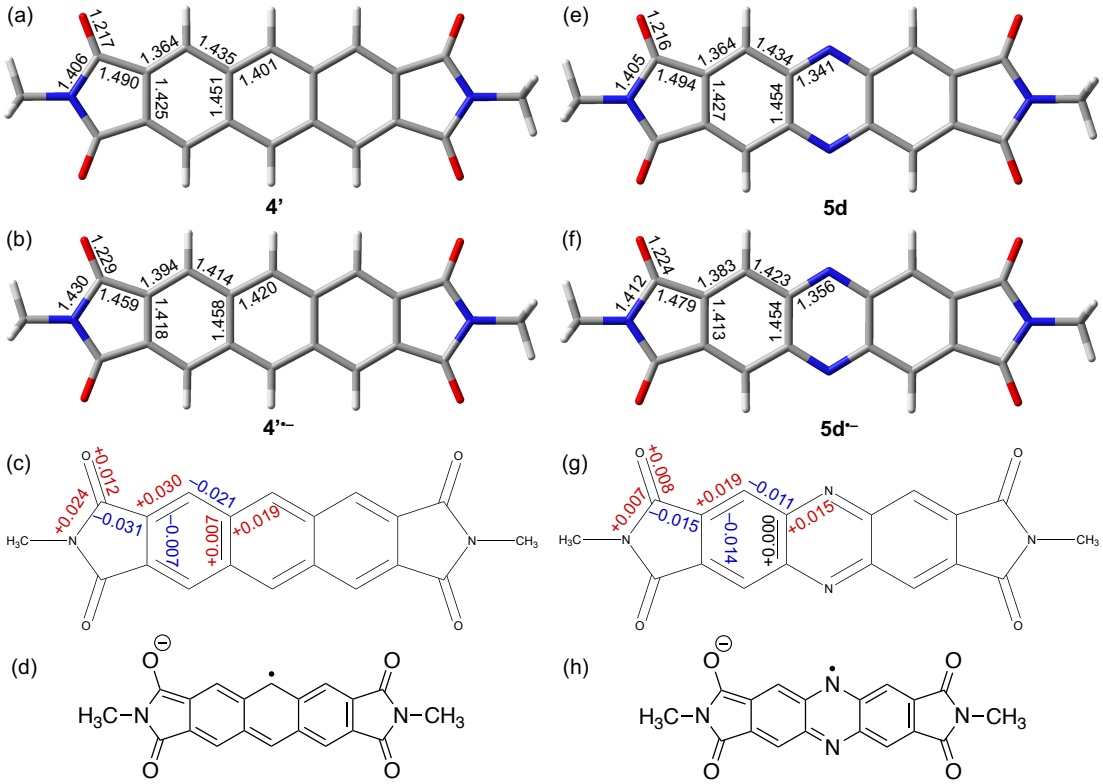

Figure S41. Optimized structures of (a) **6**, (b) **6'**$^{\bullet-}$, (e) **4**, and (f) **4**$^{\bullet-}$. The values indicate the bond lengths. (c,g) The bond lengths deviation from neutral species. (d,h) One of the resonance structures with quinoidal forms. DFT calculations were conducted at the (U)B3LYP/6-31G+(d,p) level. The substituents on the imide groups are replaced with methyl groups to simplify the calculations.

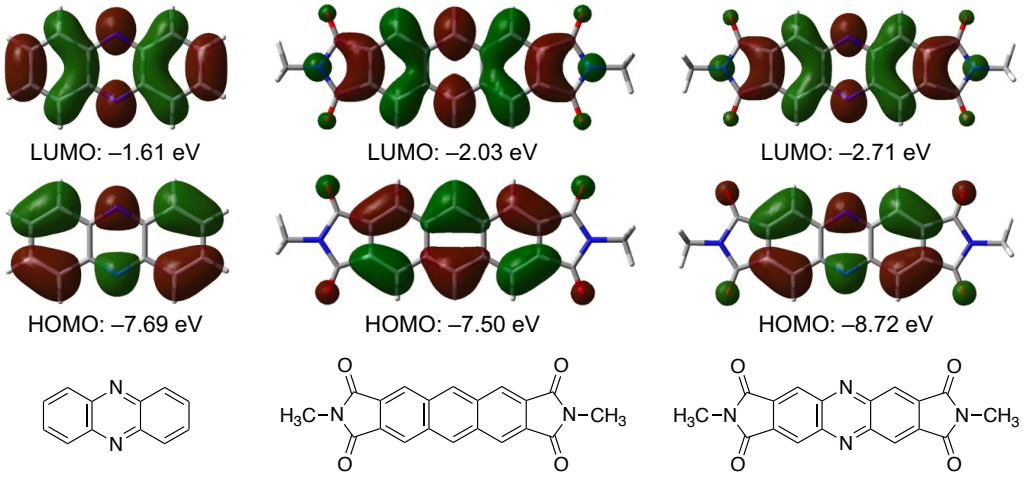

Figure S42. Calculated HOMO and LUMO levels of phenazine, anthracene diimide, and PzBI. DFT calculations were conducted at the CAM-B3LYP/6–31+G(d,p) level of theory.

Table S4. Cartesian coordinate and geometry of phenazine.

C	-0.0003312	-0.0417506	-0.0006083
C	0.0321079	-0.0756151	1.4274659
C	1.2234142	-0.1495538	2.0832419
C	2.4551425	-0.1943302	1.3600832
C	2.4658712	-0.1641047	-0.0014189
C	1.2376611	-0.0867665	-0.7274445
N	1.2618028	-0.0578137	-2.0622681
C	0.087186	0.0147315	-2.693296
C	0.054747	0.048596	-4.12137
C	-1.1365594	0.1225347	-4.7771461
C	-2.3682876	0.1673111	-4.0539875
C	-2.3790162	0.1370856	-2.6924853
C	-1.1508062	0.0597474	-1.9664599
N	-1.1749478	0.0307947	-0.6316361
H	-0.9162647	-0.040419	1.9523259
H	3.3864226	-0.1968291	-0.5738192
H	1.0031196	0.0134	-4.6462301
H	-3.2995676	0.16981	-2.1200851
H	3.3888456	-0.2530616	1.9100432
H	1.2463545	-0.1751984	3.1679186
H	-3.3019907	0.2260425	-4.6039474
H	-1.1594996	0.1481793	-5.8618228

Negative frequency = zero

Sum of electronic and thermal free energies = –571.182625 Hartree

Table S5. Cartesian coordinate and geometry of *N*,*N*′-dimethyl anthracene bisimide.

C	0	0	0
C	0	0	1.4401816
C	2.4390985	0	1.4399761
C	2.4390985	0	-0.0002055
C	3.6856693	0	2.1496556
C	3.6856545	0	-0.7099647
C	-1.2465707	0	-0.7096795
C	-1.246556	0	2.1499408
C	-2.3944503	0	0.0092883
C	-3.8116965	0	-0.4458364
C	-2.3945233	0	1.4311822
C	-3.8128576	0	1.8827163
C	4.8335489	0	1.4306877
C	6.2507951	0	1.8858125
C	4.8336218	0	0.0087938
C	6.2519562	0	-0.4427403
H	-1.2597776	0	-1.7950689
H	-1.2594883	0	3.2353498
H	3.6988761	0	3.235045
H	3.6985868	0	-1.7953737
N	7.0228471	0.0000316	0.7203775
N	-4.5837486	-0.0000144	0.7195985
O	6.6875124	0.0000221	3.0153365
O	6.6974421	0.0000222	-1.5691867
O	-4.2583436	-0.0000261	3.0091628
O	-4.2484138	-0.0000225	-1.5753605
C	8.4714504	0.0000571	0.7102149
H	8.8452607	0.8873727	0.1952161
H	8.8083924	0.0006863	1.7463062
H	8.8453577	-0.8878561	0.1963056
C	-6.0323519	-0.0000533	0.7297611
H	-6.4062099	0.8873346	1.2446026
H	-6.3692939	0.0003811	-0.3063302
H	-6.4062115	-0.8878943	1.243828
C	1.2195985	0	2.1180733
C	1.2195	0	-0.6780972
H	1.2196901	0	3.2043607
H	1.2194085	0	-1.7643846

Negative frequency = zero

Sum of electronic and thermal free energies = –1179.104671 Hartree

Table S6. Cartesian coordinate and geometry of *N*,*N*′-dimethyl PzBI.

C	-0.0017935	-0.0417472	0.0025076
C	0.005669	-0.0744981	1.436112
C	1.208526	-0.1481341	2.0532778
C	2.4361764	-0.1927539	1.3323549
C	2.4862832	-0.1646869	-0.020394
C	1.2409946	-0.0869353	-0.7272202
C	1.5380136	-0.1973398	3.5072317
C	3.5444791	-0.2701992	2.3278341
N	1.2589249	-0.0577093	-2.0605817
N	2.9287843	-0.2680066	3.5819088
O	0.7909669	-0.1818026	4.4588333
O	4.7366063	-0.324841	2.130593
C	0.0886476	0.0147286	-2.696412
C	0.0811858	0.0474792	-4.1300155
C	-1.1216715	0.1211149	-4.7471817
C	-2.3493212	0.1657347	-4.0262593
C	-2.3994278	0.1376677	-2.6735099
C	-1.1541396	0.0599163	-1.9666848
C	-1.4511589	0.1703198	-6.2011359
C	-3.4576241	0.2431804	-5.0217384
N	-1.1720697	0.0306904	-0.6333218
N	-2.8419296	0.2409864	-6.2758133
O	-0.704112	0.1547831	-7.1527373
O	-4.6497513	0.2978217	-4.824497
H	-0.9348209	-0.0399997	1.9744979
H	3.414822	-0.1981234	-0.57918
H	1.0216756	0.0129808	-4.6684016
H	-3.3279666	0.1711042	-2.114724
C	-3.5642084	0.3051739	-7.5307543
H	-3.264893	1.1923377	-8.0923399
H	-3.3520524	-0.5805658	-8.1328127
H	-4.6273191	0.3521332	-7.2974907
C	3.651063	-0.3321938	4.83685
H	3.4389266	0.5535574	5.4388987
H	3.3517291	-1.2193447	5.3984457
H	4.7141725	-0.3791773	4.6035859

Negative frequency = zero

Sum of electronic and thermal free energies = –1211.201859 Hartree

9. Optical properties

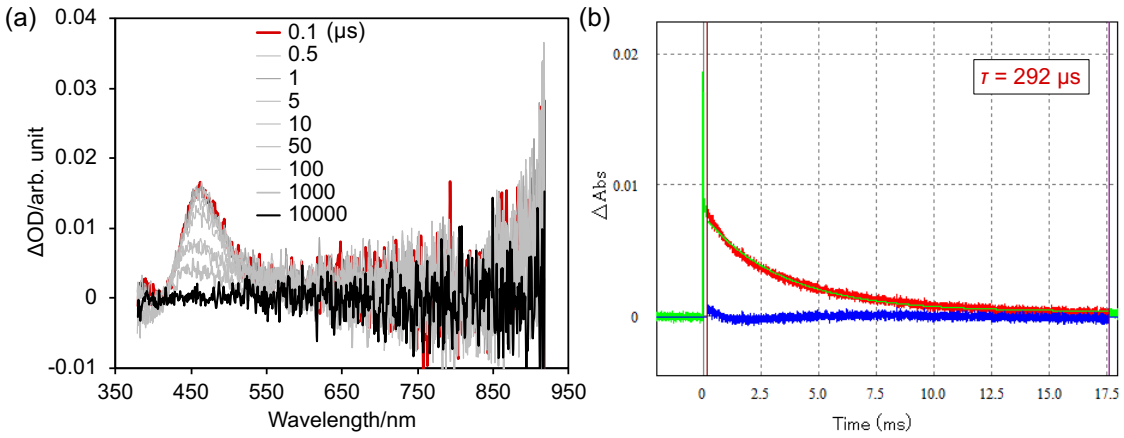

Figure S43. (a) Transient absorption spectra and (b) decay profiles of **4a** in CH_2Cl_2 under N_2.

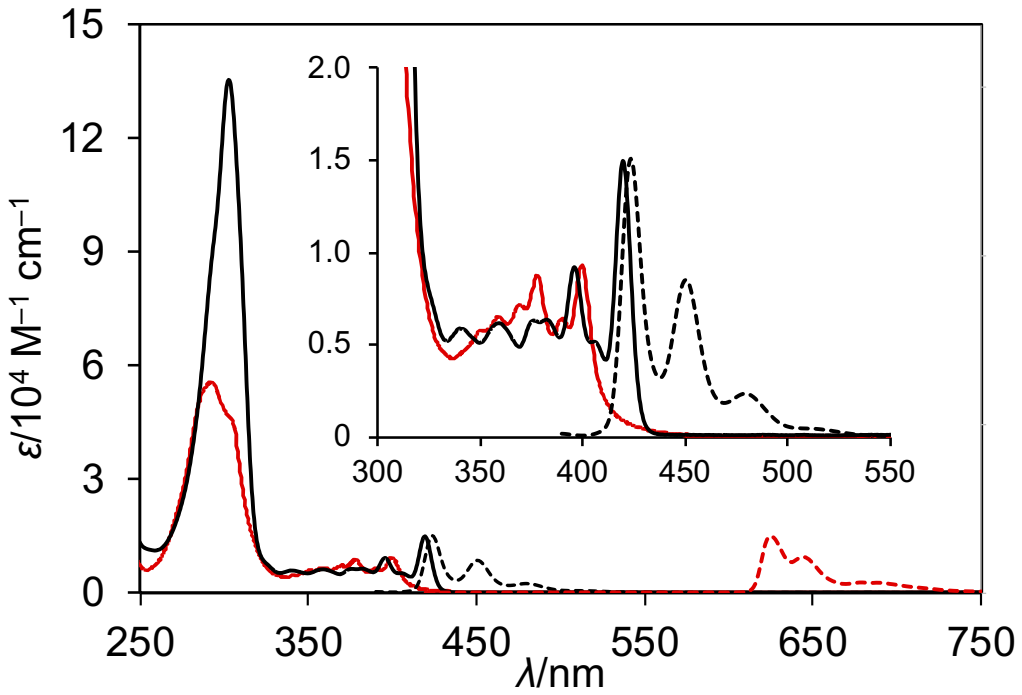

Figure S44. UV/Vis absorption and emission spectra of **4b** (red line) and **6** (black line). (**4b**: absorbance was recorded in CH_2Cl_2 at room temperature, and emission was recorded in 2-methyltetrahydrofuran at 77 K with λ_{ex} = 365 nm); (**6**: λ_{ex} = 365 nm, in CH_2Cl_2, at room temperature). λ = wavelength; ε = extinction coefficient.

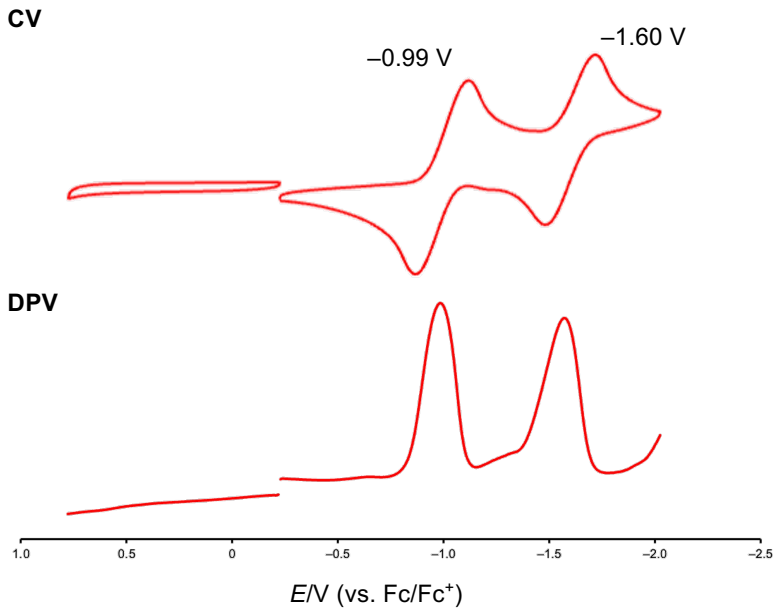

Figure S45. Cyclic and differential pulse voltammograms of **4a** in CH_2Cl_2.

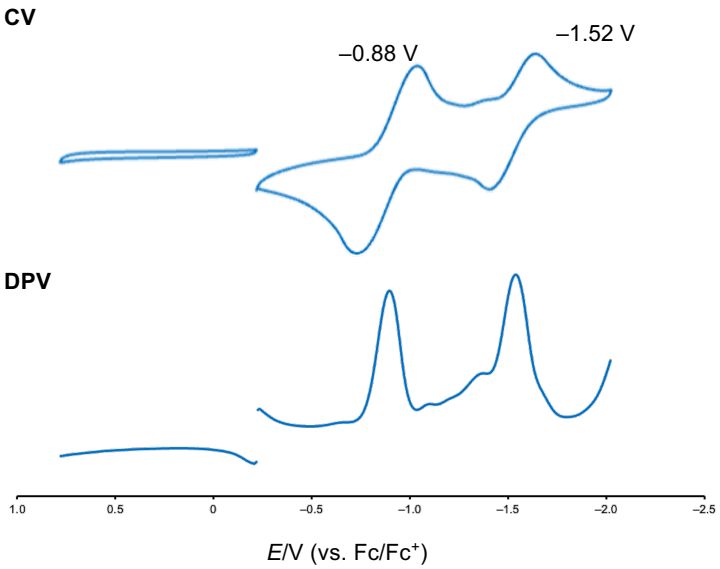

Figure S46. Cyclic and differential pulse voltammograms of **4c** in CH_2Cl_2.

11. References

1. McKinnon, J. J.; Spackman, M. A.; Mitchell, A. S. Novel Tools for Visualizing and Exploring Intermolecular Interactions in Molecular Crystals. *Acta Crystallogr. B* **2004**, *60*, 627–668.
2. *Gaussian 16*, Revision A.03, M. J. Frisch, G. W. Trucks, H. B. Schlegel, G. E. Scuseria, M. A. Robb, J. R. Cheeseman, G. Scalmani, V. Barone, G. A. Petersson, H. Nakatsuji, X. Li, M. Caricato, A. V. Marenich, J. Bloino, B. G. Janesko, R. Gomperts, B. Mennucci, H. P. Hratchian, J. V. Ortiz, A. F. Izmaylov, J. L. Sonnenberg, D. Williams-Young, F. Ding, F. Lipparini, F. Egidi, J. Goings, B. Peng, A. Petderson, D. Ranasinghe, V. G. Zakrzewski, J. Gao, N. Rega, G. Zheng, W. Liang, M. Hada, M. Ehara, K. Toyota, R. Fukuda, J. Hasegawa, M. Ishida, T. Nakajima, Y. Honda, O. Kitao, H. Nakai, T. Vreven, K. Throssell, J. A. Montgomery, Jr., J. E. Peralta, F. Ogliaro, M. J. Bearpark, J. J. Heyd, E. N. Brothers, K. N. Kudin, V. N. Staroverov, T. A. Keith, R. Kobayashi, J. Normand, K. Raghavachari, A. P. Rendell, J. C. Burant, S. S. Iyengar, J. Tomasi, M. Cossi, J. M. Millam, M. Klene, C. Adamo, R. Cammi, J. W. Ochterski, R. L. Martin, K. Morokuma, O. Farkas, J. B. Foresman, and D. J. Fox, Gaussian, Inc., Wallingford CT, **2016**.
3. Becke, A. D. Density-functional Thermochemistry. III. The Role of Exact Exchange. *J. Chem. Phys.* **1993**, *98*, 5648–5652.
4. Yanai, T.; Tew, D. P.; Handy, N. C. A New Hybrid Exchange–Correlation Functional Using the Coulomb-Attenuating Method (CAM-B3LYP). *Chem. Phys. Lett.* **2004**, *393*, 51–57.
5. Perdew, J. P.; Burke, K.; Ernzerhof, M. Generalized Gradient Approximation Made Simple. *Phys. Rev. Lett.* **1996**, *77*, 3865–3868.
6. Guha, S. K.; Obora, Y.; Ishihara, D.; Matsubara, H.; Ryu, I.; Ishii, Y. Aerobic Oxidation of Cyclohexane Using N-Hydroxyphthalimide Bearing Fluoroalkyl Chains. *Adv. Synth. Catal.* **2008**, *350*, 1323–1330
7. Yanase, T.; Tanoguchi, H.; Sakai, N.; Jin, M.; Yamane, I.; Kato, M.; Ito, H.; Nagahama, T.; Shimada, T. Single Crystal Growth of π-Conjugated Large Molecules without Solubilizing Alkyl Chains via the Naphthalene Flux Method. *Cryst. Growth Des.* **2021**, *21*, 4683–4689.
8. Takahashi, K.; Shan, B.; Xu, X.; Yang, S.; Koganezawa, T.; Kuzuhara, D.; Aratani, N.; Suzuki, M.; Miao, Q.; Yamada, H. Engineering Thin Films of a Tetrabenzoporphyrin toward Efficient Charge-Carrier Transport: Selective Formation of a Brickwork Motif. *ACS Appl. Mater. Interfaces* **2017**, *9*, 8211–8218
9. Hayakawa, S.; Matsuo, K.; Yamada, H.; Fukui, N.; Shinokubo, H. Dinaphthothiepine

Bisimide and Its Sulfoxide: Soluble Precursors for Perylene Bisimide. *J. Am. Chem. Soc.* **2020**, *142*, 11663–11668.